INTERNATIONAL JOURNAL FOR NUMERICAL METHODS IN FLUIDS
Int. J. Numer. Meth. Fluids 2001; **36**: 53–90

Three-dimensional numerical simulation of Marangoni instabilities in liquid bridges: influence of geometrical aspect ratio

M. Lappa, R. Savino* and R. Monti

Dipartimento di Scienza e Ingegneria dello Spazio 'Luigi G. Napolitano', Università degli Studi di Napoli 'Federico II', Napoli, Italy

SUMMARY

Oscillatory Marangoni convection in silicone oil–liquid bridges with different geometrical aspect ratios is investigated by three-dimensional and time-dependent numerical simulations, based on control volume methods in staggered cylindrical non-uniform grids. The three-dimensional oscillatory flow regimes are studied and compared with previous experimental and theoretical results. The results show that the critical wavenumber (m), related to the azimuthal spatio-temporal flow structure, is a monotonically decreasing function of the geometrical aspect ratio of the liquid bridge (defined as the ratio of length to diameter). For this function, a general correlation formula is found, which is in agreement with the previous experimental findings. The critical Marangoni number and the oscillation frequency are decreasing functions of the aspect ratio; however, the critical Marangoni number, based on the axial length of the bridge, does not change much with the aspect ratio. For each aspect ratio investigated, the onset of the instability from the axisymmetric steady state to the three-dimensional oscillatory one is characterized by the appearance of a standing wave regime that exhibits, after a certain time, a second transition to a travelling wave regime. The standing wave regime is more stable for lower aspect ratios since it lasts for a long time. This behaviour is explained on the basis of the propagation velocity of the disturbances in the liquid phase. For this velocity, a general correlation law is found as a function of the aspect ratio and of the Marangoni number. Copyright © 2001 John Wiley & Sons, Ltd.

KEY WORDS: liquid bridge; Marangoni flow; Navier–Stokes calculations

1. INTRODUCTION

Considerable attention has been paid in recent years to surface tension-driven (Marangoni) convection in liquid floating zones and similar configurations under microgravity conditions. The reason for this interest is that once buoyancy convection is reduced by several orders of magnitude in space, surface tension-driven flows are the only mechanisms responsible for the

* Correspondence to: Dipartimento di Scienza e Ingegneria dello Spazio 'Luigi G. Napolitano', Università degli Studi di Napoli 'Federico II', P. le V. Tecchio 80, 80125 Napoli, Italy.

Received July 1999
Revised May 2000

appearance of undesirable instabilities in liquid semiconductors or other liquid melts materials during container-less floating zone crystal growth methods.

For a better understanding and optimization of these processes, model problems have been formulated and studied analytically, numerically and experimentally. The most common model is that of the half zone consisting of two circular coaxial disks at different temperatures, with a bridge of liquid suspended between them. Since the end of 1970s, Chun and West [1,2] have shown on ground experiments with small size half zones and high-Prandtl number liquids ($Pr \gg 1$) that the Marangoni convection in liquid bridges heated from above or below shows a transition from a steady axisymmetric toroidal flow to a three-dimensional oscillatory flow when a critical temperature difference between the liquid bridge supports is exceeded. Preisser *et al.* [3], Velten *et al.* [4] and Frank and Schwabe [5] undertook studies on ground research over a large range of experimental conditions. They found that the oscillatory Marangoni flow exhibits different behaviours depending on the Prandtl number of the liquid employed and on the geometrical aspect ratio of the zone, defined as the ratio of the length L and of the diameter D of the bridge ($A = L/D$).

Monti [6] investigated the onset of instability of Marangoni convection in space by using large liquid bridges with lengths of the order of several centimetres and in the absence of buoyancy effects.

Recent experimental works have been performed by Petrov *et al.* [7], Muehlner *et al.* [8] and Schwabe *et al.* [9].

In the last years the development of supercomputers and efficient numerical methods has led the investigators to study the problem through numerical solution of the three-dimensional and time-dependent Navier–Stokes equations.

Rupp *et al.* [10] studied the instability behaviour by three-dimensional numerical simulations for liquids with different Prandtl numbers and for a fixed aspect ratio ($A = 0.6$).

Stability analyses were carried out by several authors [11–18,25] to define, in the non-dimensional parameter space, sufficient conditions for stability and instability.

The most complete results on the subject are those reported in the linear stability analyses of Kuhlmann [15], Kuhlmann and Rath [16], Chen and Roux [17] and Chen and Hu [18]. The basic axisymmetric Marangoni flow was obtained by numerical solutions of the Navier–Stokes equations, together with the appropriate boundary and symmetry conditions, and the eigenvalue problem for the three-dimensional disturbances was solved over a range of Prandtl numbers and for aspect ratios close to unity. These results predicted the critical Marangoni numbers and the form of the most dangerous disturbances, characterized by the appropriate value of the critical wavenumber, in the neighbourhood of the neutral stability point (i.e. at the onset).

Kuhlmann and Rath [16] found that the three-dimensional supercritical state after the Hopf bifurcation point is given by a superposition of two counter-propagating hydrothermal waves, with axial and azimuthal components. If the two waves have equal amplitude, the resulting disturbance is a 'standing wave', with the minimum and maximum disturbances pulsating at fixed azimuthal positions; while the superposition of waves with different amplitude gives rise to a 'travelling wave', with the minimum and maximum disturbances travelling in the azimuthal direction. Unfortunately, nothing can be predicted by the linear stability analyses about the amplitude of these disturbances.

The experiments performed on ground and in microgravity conditions revealed one or the other instability mechanism. For instance, the travelling wave has been observed by Chun and West [1], Preisser *et al.* [3], Frank *et al.* [5], Monti [6], Muehlner *et al.* [8] and Schwabe *et al.* [9]. The standing wave, instead, has been observed during experimental ground-based activities (Velten *et al.* [4], Frank *et al.* [5]).

Recent numerical results obtained by Savino and Monti [19] and Monti *et al.* [20] have shown that the standing wave and the travelling wave models correspond to two consecutive transitions of the Marangoni flow. In particular, for large-Prandtl number liquids the flow exhibits a first transition from the axisymmetric steady state to the three-dimensional oscillatory state, characterized by the standing wave instability and, after a certain time, a second transition from the standing wave to the travelling wave. These results for a liquid bridge with a fixed aspect ratio ($A = 1$) have also been validated by experimental results on the ground (Monti *et al.* [21]), where, for the first time, the transition from one regime to the other was clearly observed.

In a previous work [22] a parallel solution numerical method was introduced and applied to study three-dimensional Marangoni flow instabilities in liquids with low Prandtl number.

In this paper, the method is extended to high Prandtl numbers for which most of the existing information comes from experiments and linear stability calculations. In particular, the attention is focused on the influence of the aspect ratio on the flow instability, on the critical wavenumber (m) and on the spatio-temporal structures (pulsating or rotating).

2. PHYSICAL AND MATHEMATICAL MODEL

2.1. Basic assumptions

Figure 1 shows the geometry of the problem and the boundary conditions. A cylindrical liquid bridge is suspended between two coaxial disks with constant temperatures ($\bar{T} = \bar{T}_0 \pm \Delta T/2$), where $\bar{T}_0$ is the ambient temperature and ΔT is the overall temperature difference.

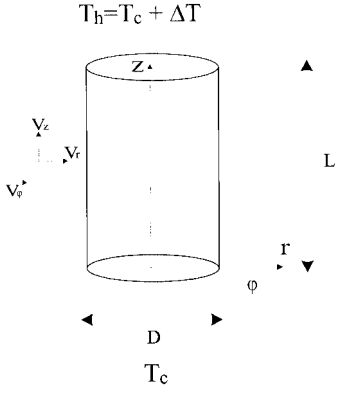

Figure 1. Scheme of the liquid bridge.

The liquid is assumed homogeneous and Newtonian, with constant density and transport coefficients. The bridge is bounded by a cylindrical and undeformable liquid–gas interface, with a surface tension σ exhibiting a linear decreasing dependence on the temperature

$$\sigma = \sigma_0 - \sigma_T(\bar{T} - \bar{T}_0) \tag{1}$$

where σ_0 is the surface tension for $\bar{T} = \bar{T}_0$; σ_T is the negative rate of change of the surface tension with temperature ($\sigma_T = -\mathrm{d}\sigma/\mathrm{d}\bar{T} > 0$).

The hypothesis of rigid free surface is acceptable if zero-g conditions prevail or, on the ground, if the volume of the liquid bridge is small and if the geometrical aspect ratio is sufficiently low.

2.2. Non-dimensional field equations and boundary conditions

With the above assumptions the flow is governed by the continuity Navier–Stokes and energy equations, which in non-dimensional conservative form read

$$\underline{\nabla} \cdot \underline{V} = 0 \tag{2a}$$

$$\frac{\partial \underline{V}}{\partial t} = -\underline{\nabla} p - \underline{\nabla} \cdot [\underline{V}\underline{V}] + Pr \nabla^2 \underline{V} \tag{2b}$$

$$\frac{\partial T}{\partial t} = -\underline{\nabla} \cdot [\underline{V} T] + \nabla^2 T \tag{2c}$$

where V, p and T are the non-dimensional velocity, pressure and temperature respectively; Pr is the Prandtl number, defined by $Pr = \nu/\alpha$ (ν is the kinematic viscosity and α is the thermal diffusivity). The non-dimensional form results from scaling the lengths by the axial distance between the circular disks (L) and the velocity by the energy diffusion velocity $V_\alpha = \alpha/L$; the scales for time and pressure are L^2/α and $\rho\alpha^2/L^2$ respectively. The temperature, measured with respect to the initial temperature $\bar{T}_0$ is scaled by (ΔT)

$$T = (\bar{T} - \bar{T}_0)/(\Delta T) \tag{3}$$

The initial conditions are

$$t = 0: \quad \underline{V}(z, r, \varphi) = 0, \qquad T(z, r, \varphi) = 0 \tag{4}$$

i.e. the liquid is motionless and at ambient temperature.

For $t > 0$, the boundary conditions are the non-slip conditions and the condition of prescribed temperatures on the circular disks, the kinematic condition of stream surface (zero normal velocity), the Marangoni conditions (shear stress balance) and the adiabatic condition on the cylindrical interface:

on the cold disk

$0 \le r \le R/L;\ 0 \le \varphi \le 2\pi$

$$\underline{V}(z=0, r, \varphi, t) = 0; \qquad T(z=0, r, \varphi, t) = -\frac{1}{2} \tag{5}$$

on the hot disk
$0 \le r \le R/L;\ 0 \le \varphi \le 2\pi$

$$\underline{V}(z=1, r, \varphi, t) = 0; \qquad T(z=1, r, \varphi, t) = \frac{1}{2} \tag{6}$$

on the cylindrical free surface
$0 \le z \le 1;\ 0 \le \varphi \le 2\pi$

$$V_r\left(z, r=\frac{R}{L}, \varphi, t\right) = 0 \tag{7a}$$

$$\frac{\partial V_z}{\partial r}\left(z, r=\frac{R}{L}, \varphi, t\right) = -Ma\,\frac{\partial T}{\partial z}\left(z, r=\frac{R}{L}, \varphi, t\right) \tag{7b}$$

$$r\,\frac{\partial V_\varphi}{\partial r}\left(z, r=\frac{R}{L}, \varphi, t\right) - V_\varphi\left(z, r=\frac{R}{L}, \varphi, t\right) = -Ma\,\frac{\partial T}{\partial \varphi}\left(z, r=\frac{R}{L}, \varphi, t\right) \tag{7c}$$

$$\frac{\partial T}{\partial r}\left(z, r=\frac{R}{L}, \varphi, t\right) = 0 \tag{7d}$$

where the reference Marangoni number Ma is defined as $Ma = \sigma_T(\Delta T)L/\mu\alpha$.

3. NUMERICAL SOLUTION

3.1. Solution method

Equations (2a)–(2c) and the initial and boundary conditions (4)–(7) were solved numerically in cylindrical co-ordinates in primitive variables by a control volume method. The domain was discretized with a non-uniform but structured axisymmetric mesh and the flow field variables defined over a staggered grid.

The axial velocity component V_z is staggered in the axial direction with respect to the point in which temperature and pressure are computed. In a similar way the radial and azimuthal velocity components are staggered in the radial and the azimuthal directions respectively (see Figure 2).

The finite volume approach relies directly on the application of the integral form of balance laws. Thus, the conservation laws have been written for an arbitrary spatial domain Ω bounded by a surface $\partial\Omega$. Since the collocation of the variables on the grid is staggered, each

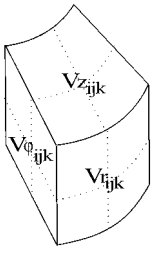

Figure 2. Collocation of the variables on the computational grid.

variable is characterized by a different control volume; see Figure 3, where the projection (over a generic meridian plane) of the control volume Ω_{V_z} for the axial velocity, Ω_{V_r} for the radial velocity and Ω_p for the pressure and the temperature is shown (the control volumes for p and T are the same; the control volume for the azimuthal velocity V_φ is shifted of an angular co-ordinate $\Delta\varphi/2$ in the azimuthal direction with respect to the control volume used for p and T). Integrating over the generic control volume and using the Gauss theorem to transform volume integrals in surface integrals, the equations read

$$\underline{V}^{n+1} = \underline{V}^n + \Delta t \frac{1}{\Omega}\left[-\int_{\partial\Omega} [\underline{V}\underline{V}]\cdot\underline{n}\, \mathrm{d}S + Pr \int_{\partial\Omega} [\underline{\nabla}\underline{V}]\cdot\underline{n}\, \mathrm{d}S \right]^n - \Delta t \frac{1}{\Omega}\int_\Omega \underline{\nabla} p^n \, \mathrm{d}\Omega \tag{8a}$$

$$T^{n+1} = T^n + \Delta t \frac{1}{\Omega}\left[-\int_{\partial\Omega} [\underline{V}T]\cdot\underline{n}\, \mathrm{d}S + \int_{\partial\Omega} [\underline{\nabla}T]\cdot\underline{n}\, \mathrm{d}S \right]^n \tag{8b}$$

The problem is solved with the well-known marker-and-cell method (see e.g. Lappa and Savino [22] and Fletcher [23]).

3.2. Validation of the numerical procedure

In this section the numerical model is validated by quantitative comparisons with two-dimensional numerical results and with existing three-dimensional linear stability results for Prandtl numbers as close as possible to those used in the present work.

For two-dimensional computations, the streamfunction minimum of the axisymmetric flow in the case $A = 0.5$, $Pr = 10$ and $Ma = 1000$ is compared with the results reported by Kuhlmann and Rath [16] and Wanschura *et al.* [25]. A very good agreement is obtained between the values obtained with the present code and those by Kuhlmann and Rath [16] and Wanschura *et al.* [25], as shown in Table I(a) and (b).

To check that the code is able to 'capture' the physical instabilities of Marangoni flow, critical Marangoni numbers have been computed and compared with the results of two different available stability analyses. In particular, the cases $A = 0.6$ and $Pr = 10$ (reported in the recent linear stability analysis of Chen and Hu [18]) and $A = 0.5$, $Pr = 4$ (reported in the linear stability analysis of Wanschura *et al.* [25]) have been considered.

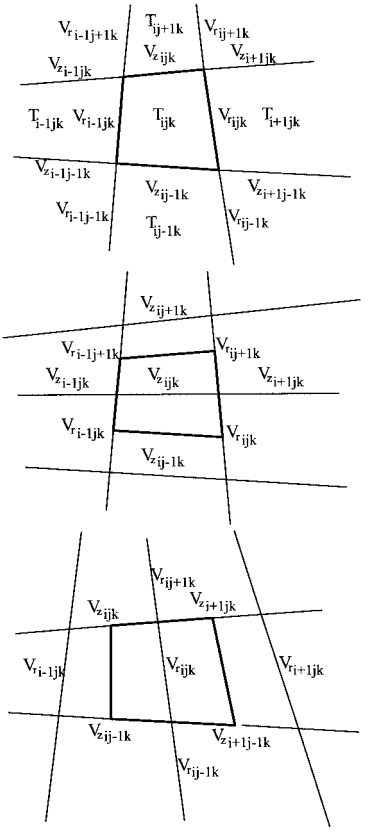

Figure 3. Control volumes adopted for the different variables.

Regarding the definition of the critical conditions for the onset of instability, it is important to clarify the criterion adopted to evaluate so-called critical Marangoni number.

The linear stability analyses assume that the critical Marangoni number Ma_c is a threshold value of the Marangoni number at which the growth rate of the disturbances is zero. Typically, in these analyses the critical Marangoni number is computed using an extrapolation of the growth rate to zero.

For the present calculations, the critical Marangoni numbers have been defined as those for which the disturbance amplitude becomes vanishing (i.e. the non-dimensional azimuth velocity is of the order of 10^{-2}) but is still characterized by a well-defined frequency. These values have been determined using three-dimensional simulation rather than extrapolation.

For $Pr = 10$ and $A = 0.6$ the linear stability analysis predicts $Ma_c = 13000$ (using as reference length the length L of the bridge, according to the present non-dimensionalization). The critical Marangoni number determined by the present numerical computations is

Table I. Minimum streamfunction of the axisymmetric flow as a function of mesh spacing.

Grid size	Minimum streamfunction
(a) Uniform grids	
Kuhlmann and Rath [16]	−4.1
Wanschura *et al.* [24] 25×14	−4.08
Wanschura *et al.* [24] 50×50	−4.10
Present results 20×20	−4.03
Present results 24×24	−4.075
Present results 30×30	−4.094
Present results 40×40	−4.10
Present results 50×50	−4.103
(b) Non-uniform grids	
Present results 24×24	−4.075
Present results $24\times(20+4)$	−4.077
Present results $24\times(18+6)$	−4.085
Present results $24\times(16+8)$	−4.10
Present results $24\times(14+10)$	−4.102

$Ma_c \cong 13400$ (3 per cent greater that the linear stability value) with $m=1$ and a pulsating regime that is stable for a long time.

For $Pr=4$ and $A=0.5$, Wanschura *et al.* [25] predict $m=2$ and $Ma_c \cong 4200$. The present results give $Ma_c \cong 4400$ (5 per cent greater that the linear stability value) and a pulsating regime that develops into a travelling regime after a short transient time.

These comparisons provide a sufficient validation of the present numerical code.

3.3. Grid refinement study

In this sub-section, in order to show the numerical convergence of the present algorithm, a grid refinement study is presented.

In Table I(a) and (b) the computed minimum streamfunction is shown for different grid sizes. The computations have been performed for uniform grids $N_z \times N_r$ (the first number denotes the number of collocation points in the axial direction and the second defines the grid size in the radial direction) and for non-uniform grids. For the latter a finer grid has been introduced near the free surface to locally enhance the resolution. This zone plays a 'critical role' in the computations since a Marangoni boundary layer is present here. It is characterized by extremely steep radial gradients of velocity and temperature induced by the driving force acting on the free surface. The number of points clustered near the free surface are specified in Table I(b) using the notation $N_z \times (N_{r_b} + N_{r_s})$ (where N_{r_s} is the number of points stretched near the free surface and N_{r_b} is the number of points uniformly distributed in the bulk over a radius $R_b = 0.7R$). The N_{r_s} points near the free surface are clustered using the stretching function (s) due to Roberts and Eiseman (for further details see Fletcher [23]; for the present computations, the stretching control parameters $\mathscr{P}=1$ and $\mathscr{Q}=2$ have been used). This

corresponds to a grid-stretching factor δ not constant with a maximum value (δ_{max}) for the layer of points adjacent the free surface.

Wanschura *et al.* [25] found a change of less than 1 per cent in the streamfunction for a resolution of 25×14 points. In the present paper, the same accuracy has been reached using uniform grids for a resolution of 24×24 points.

Table I(b) shows the results obtained with the present code using a grid size of 24 points in the axial direction and a total of 24 points in the radial direction. It can be seen that a non-uniform mesh with $24 \times (16 + 8)$ points gives the same accuracy as a uniform mesh with 40×40 points. This trend is confirmed by the behaviour of the axial component of velocity (at $z = 0.5$ and different radial positions) shown in Table II.

A grid refinement study has been conducted also on the influence of the number of points used in the azimuthal direction. In this case, the criterion for grid convergence is that the oscillation frequency changes less than 4 per cent. The case $A = 0.5$, $Pr = 4$ and a supercritical situation ($Ma = 4800$) has been considered to verify the accuracy of the simulation since it is expected that in this situation the numerical dissipation might be strong. Table III(a) shows that for the case $A = 0.5$ grid convergence can be obtained using 20 points in the azimuthal direction.

Table II. Axial velocity of the axisymmetric flow at $z = 0.5$ and at different radial positions as a function of grid spacing.

Grid size	u at $r = 0.25$	u at $r = 0.5$	u at $r = 1.0$
20×20	14.665	16.60	-43.83
24×24	14.59	16.624	-43.82
30×30	14.504	16.622	-43.80
40×40	14.44	16.605	-43.77
$24 \times (16+8)$	14.446	16.58	-43.79

Table III. Three-dimensional refinement study for (a) $A = 0.5$, $Pr = 4$, $Ma = 4800$ and (b) $A = 0.2$, $Pr = 30$, $Ma = 4.0 \times 10^4$.

Grid size	f
(a)	
$24 \times (16+8) \times 20$	75.47
$24 \times (16+8) \times 25$	78.4
$24 \times (16+8) \times 30$	80
	$f \times 10^{-2}$
(b)	
$22 \times (14+14) \times 20$	14.02
$22 \times (14+14) \times 25$	14.23
$22 \times (14+14) \times 30$	14.35
$22 \times (14+14) \times 40$	14.42

4. RESULTS AND DISCUSSION

A parametric numerical analysis has been performed considering liquid bridges with different aspect ratios (from $A = 0.2$ to $A = 0.7$).

Due to the considerable computation time involved (each case requires a CPU time of the order of 100 CPU hours on a Silicon Graphics Power Challenge super computer) the investigation has been restricted to only one value of the Prandtl number ($Pr = 30$, corresponding to a silicone oil with a kinematic viscosity $v = 2 \times 10^{-6}$ m^2 s^{-1}).

According to the grid refinement study presented in the previous section, different non-uniform grids have been used to adequately meet the special features of the Marangoni flow in the liquid bridge. For high aspect ratios ($A > 0.5$) the computational points have been distributed almost uniformly in the computational domain, whereas for low aspect ratios ($A < 0.5$) finer grids have been introduced near the free surface to enhance the resolution in the thin Marangoni boundary layer.

For $A = 0.7$, 30 points have been collocated in the axial direction; this number has been reduced when reducing the length of the liquid bridge (24 for $A = 0.5$ and 22 for $A = 0.2$). In the radial direction, 30 points have been used for the case $A = 0.7$ (no stretching and $\delta = 1$ everywhere), $24 = 16 + 8$ for $A = 0.5$ ($\delta_{\max} = 1.1$) and $28 = 14 + 14$ for $A = 0.2$ ($\delta_{\max} = 1.2$) (i.e. the number of points clustered near the free surface has been increased when the aspect ratio is decreased). In particular, in the azimuthal direction, 20 points have been used for $0.4 \leq A \leq 0.7$, 30 for $0.25 \leq A \leq 0.3$ and 40 for $A = 0.2$ (for this case a grid refinement study is shown in Table III(b); the computed frequency shows grid convergence for $N_\varphi = 25$).

Figure 4(a) shows the temperature profile at the point ($z = 0.75$, $r = 0.5/2A$, $\varphi = 0$) for $A = 0.5$ ($Ma = 3.5 \times 10^4$). The spatial symmetry of the flow breaks and a transient unsteady phase develops until a stable supercritical oscillatory three-dimensional state is reached.

Very regular oscillations of the temperature are observed, with oscillation amplitudes increasing with time until a fully established oscillatory regime (with constant maxima and minima) is reached.

This behaviour is in agreement with the previous stability analyses and with the experimental results that, for large Prandtl numbers, show that the onset of Marangoni instability develops as a Hopf bifurcation.

The oscillatory behaviour of the field is strictly correlated to the breaking of the space symmetry, since at the onset of the instability an oscillatory azimuthal velocity component appears.

Figure 4(c) shows the time evolution of the azimuthal component of the velocity for $Ma = 2.2 \times 10^4$; it is very small (10^{-4} of the total velocity) and it increases with time with a very slow rate (very close to zero). Figure 4(b) shows the evolution of the azimuthal velocity for the same aspect ratio but for $Ma = 3.5 \times 10^4$. In this case the azimuthal velocity component is of the same order of magnitude of the axial and radial components.

4.1. Description of the spatial organization in the supercritical state

The computations pointed out that the temperature and the velocity fields in the supercritical state can be interpreted, at a fixed time, as the superposition of a sinusoidal, azimuthal disturbance to the steady axisymmetric field, i.e.

$$F(z, r, \varphi, t) = F_0(z, r) + \tilde{F}(z, r) \sin(m\varphi) \tag{9}$$

where m is the azimuthal wavenumber that represents the number of spatial periods in the azimuthal direction. From a fluid dynamic point of view this corresponds, for a fixed time, to a sinusoidal distortion of the section and of the axis of the three-dimensional Marangoni toroidal convection roll in the azimuthal direction. The disturbances $\tilde{F}(z, r)$ may be imagined as a distortion wound around the core of the toroidal vortex with the number of turns given by m.

To compare the present results with those obtained by previous stability analyses, the three-dimensional oscillatory disturbances were computed subtracting the azimuthally averaged flow $[F_0(z, r)]$ from the computed three-dimensional solution $F(z, r, \varphi)$.

Table IV shows that the azimuthal wavenumber of the critical mode (m) is a function of the aspect ratio of the liquid bridge. In particular, the critical number is $m = 1$ for $A \geq 0.52$, whereas higher values have been found for lower aspect ratios. Table IV shows that $m = 1$ for $A \geq 0.52$, $m = 2$ for $0.3 \leq A < 0.52$, $m = 3$ for $A = 0.25$ and $m = 4$ for $A = 0.2$ (very short liquid bridge).

The flow structure of the supercritical state is related to the value of m and hence depends on the value of the aspect ratio. The higher m is, the more complex the flow organization.

Figures 5–8 show for each aspect ratio the flow field in the cross-section orthogonal to the liquid bridge axis (a), the temperature distribution (b) and the temperature disturbances (c) in the same section and the temperature disturbances on the liquid bridge surface (d).

The (a)s in the Figures 5–8 show that in the azimuthal direction there are $2m$ convective cells driven by the surface temperature distribution (d) (each surface spot has an angular extension of $360/2m°$); the (b)s show that the isotherms of the supercritical state in the generic section z describe in this plane well-defined curves, whose shape is related to the value of the azimuthal wavenumber.

For $m = 1$, as shown by Figure 5, corresponding to the case $A = 0.7$ and $Ma = 3.35 \times 10^4$ in the generic cross-section orthogonal to the liquid bridge axis, there are two azimuthal convective cells and two thermal spots in the section and on the liquid bridge surface; moreover, the isolines of the temperature field in Figure 5(b) permit identification of a lower temperature inner region, whose shape is circular but whose position is eccentric to the geometrical axis of symmetry of the liquid bridge. In this case the supercritical flow appears as an inclined toroidal vortex (see Preisser *et al.* [3]). For $m = 2$ there are four convective cells and four thermal spots in the section and on the free surface (two hot and two cold); the inner region in this case is not circular but approximately elliptic; this is shown in Figure 6 corresponding to $A = 0.5$ and $Ma = 3.5 \times 10^4$. This elliptic region has axes e_1 and e_2 and is not eccentric but has a centre corresponding to the geometrical axis of symmetry of the liquid bridge (see Figure 6(b)). For $m = 3$ and $m = 4$ there are six and eight vortex cells and surface spots respectively, as shown in Figure 7 for $A = 0.25$ and $Ma = 3.8 \times 10^4$ and in Figure 8 for $A = 0.2$ and $Ma = 3.9 \times 10^4$. Moreover, more complicated non-eccentric patterns appear in the temperature field. For $m = 3$ the inner region has the form of a triangle, whereas for $m = 4$ it is a quadrangle.

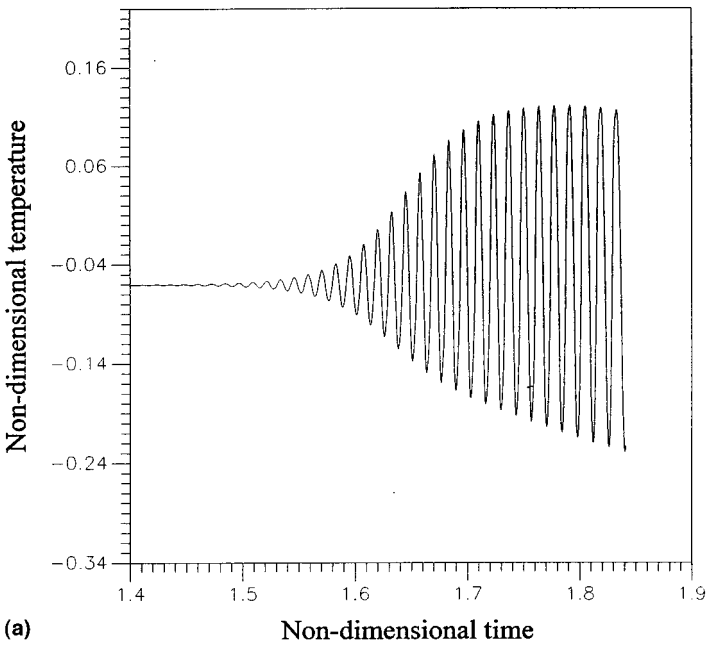

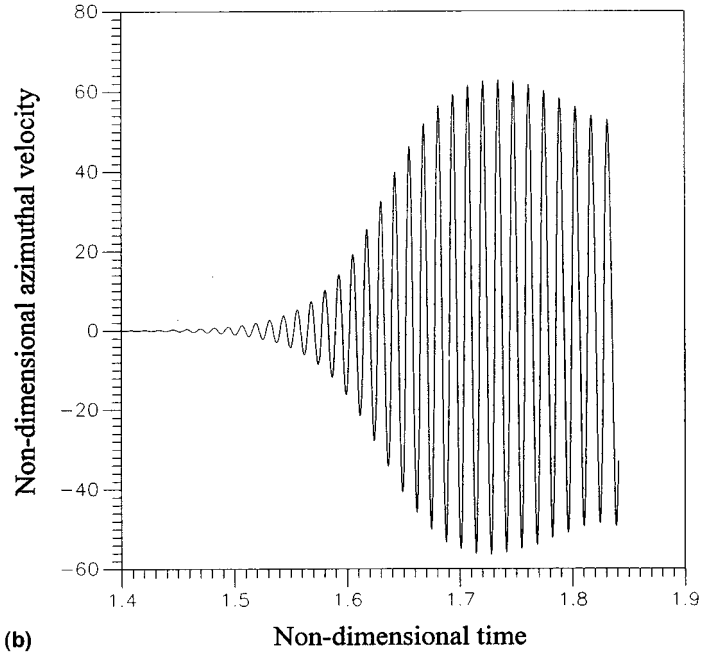

Figure 4. (a) Temperature oscillations and (b) azimuthal velocity at the point $z = 0.75$, $r = 0.5$, $\varphi = 0$ for $A = 0.5$ ($Ma = 3.5 \times 10^4$); (c) azimuthal velocity at the point $z = 0.75$, $r = 0.5$, $\varphi = 0$ for $A = 0.5$ ($Ma = 2.2 \times 10^4$).

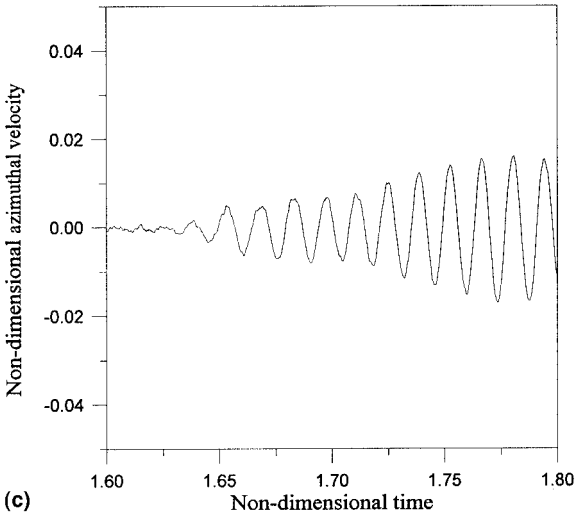

Figure 4 (*Continued*)

The behaviour of the temperature field can be related directly to the nature of the disturbances. The temperature disturbances have m maxima (minima) in the azimuthal direction (as shown in the (c)s of Figures 5–8). The nodes of the geometrical patterns described above simply correspond to these extrema in the temperature field. For $m = 2$ the geometrical pattern is an ellipse since there are two minima and two maxima (in Figure 6(b) the axes e_1 and e_2 connect, respectively, the axis of symmetry of the bridge with the positions corresponding to a minimum and to a maximum of the temperature disturbance distribution shown in Figure 6(c). For $m = 3$ and $m = 4$ the nodes correspond to the maxima of the disturbances.

The radial position of the nodal lines of the temperature perturbations also corresponds to the position of the vortex centreline after the bifurcation. The present results pointed out (in

Table IV. Ma_c versus geometrical aspect ratio.

A	Ma_c	m	$f \times 10^{-2}$	$V_p \times 10^{-2}$
0.2	2.45×10^4	4	11.36	8.91
0.25	2.4×10^4	3	7.38	7.72
0.3	2.35×10^4	2	5.17	8.12
0.4	2.3×10^4	2	3.08	4.83
0.5	2.2×10^4	2	2.77	4.35
0.52	2.17×10^4	1	2.4	7.54
0.55	2.15×10^4	1	2.25	7.06
0.6	2.1×10^4	1	2.0	6.28
0.7	2.0×10^4	1	1.65	5.18

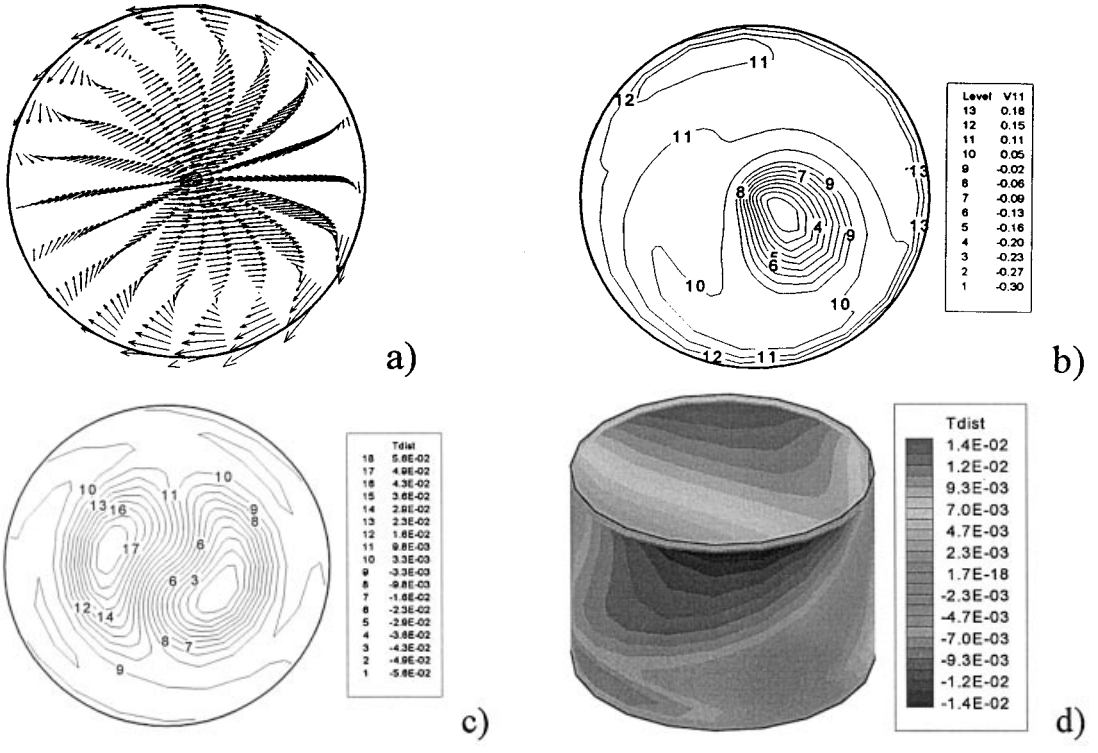

Figure 5. (a) Velocity field in the section $z = 0.5$, (b) temperature distribution and (c) temperature disturbances in the section $z = 0.75$ for $A = 0.7$; (d) temperature disturbance on the bridge surface for $A = 0.7$ ($Ma = 3.35 \times 10^4$).

agreement with previous experimental results [1–3]) that the position of the vortex core is deformed and in particular displaced sinusoidally along the perimeter of the toroidal convection roll. This is due to the occurrence of additional convective cells in the sections orthogonal to the bridge axis (shown in the (a)s of Figures 5–8), driven by the surface temperature spots (shown in the (d)s of Figures 5–8), which convect fluid in the azimuthal direction. The position of the vortex centreline describes in the space a sine curve having m maxima and m minima in the z-direction. The numerical simulations show that the part of the toroidal vortex that is displaced downwards is also displaced towards the centre of the zone and the part that is displaced away from the centre is at the same time displaced upwards (the displacement up and down is coupled to displacement out and in respectively). For this reason each plane orthogonal to the axis of symmetry shows temperature nodes that correspond to the intersection of the distorted vortex centreline with the considered plane.

For a more detailed description of the behaviour of the thermofluid dynamic field it is necessary to distinguish even critical wavenumbers from odd ones.

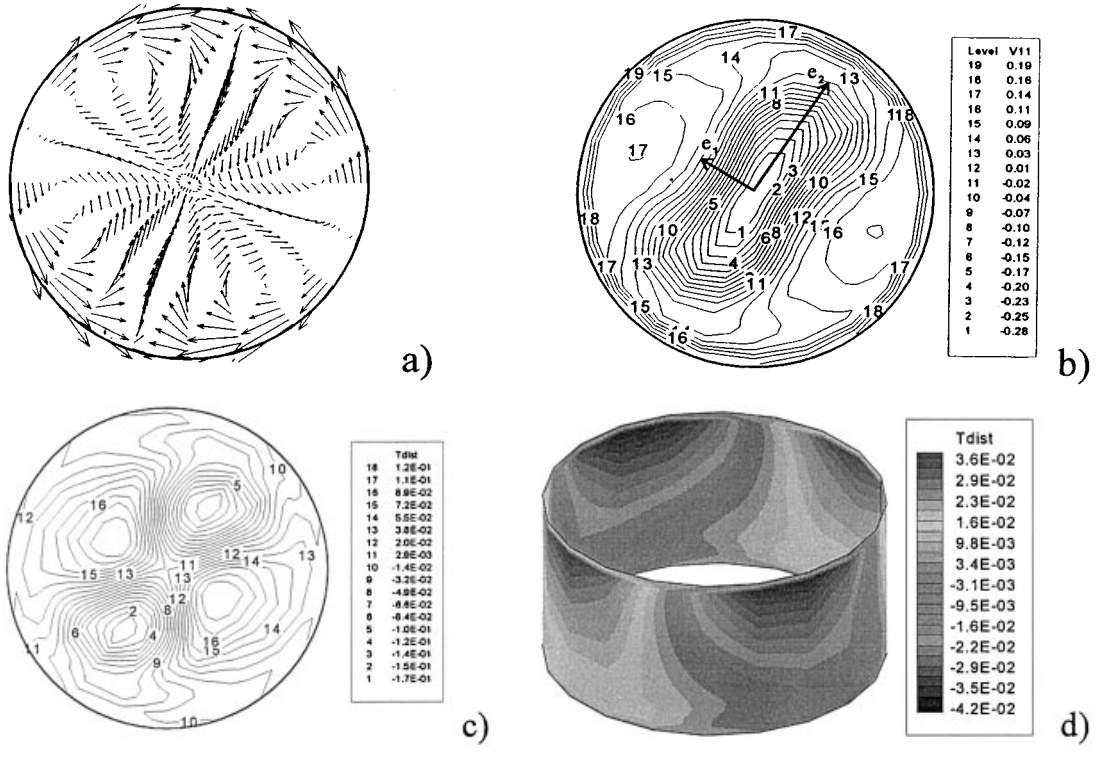

Figure 6. (a) Velocity field in the section $z = 0.5$, (b) temperature distribution, and (c) temperature disturbances in the section $z = 0.75$ for $A = 0.5$; (d) temperature disturbance on the bridge surface for $A = 0.5$ ($Ma = 3.5 \times 10^4$).

Wavenumbers $m = 1$ and $m = 3$ belong to the class of 'asymmetrical' modes; $m = 2$ and $m = 4$ are 'symmetric' modes. More generally, when the critical disturbance number (m) is odd, there are two asymmetrical vortex cells in each meridian plane of the liquid bridge.

The vortex in one half of the zone section appears smaller than the opposite vortex. The time dependence is observed as periodical interchange of the shape of the vortices in the left and right parts of the zone. After one half of the oscillation period the small vortex and the large vortex change position. The branching streamline of the opposite vortices changes its inclination continuously during an oscillation period when the azimuthal wavenumber is odd. This behaviour is illustrated in Figure 9 ($m = 1$), where the streamlines of the projected velocity vectors in the meridian plane $\varphi = 0$ are shown for eight subsequent moments in time during one cycle for the case $A = 0.7$ (the period τ has been divided into eight parts and the velocity field is shown in Figure 9(a)–(h) corresponding to $t = 0$, $\tau/8$, $\tau/4$, $3\tau/8$, $\tau/2$, $5\tau/8$, $3\tau/4$, $7\tau/8$). It can be seen that the characteristic sign of a mode $m = 1$ is a reciprocal variation of the diameters of the convection rolls on the left side and on the right side, i.e. when the left roll puffs up, the right roll contracts during half period and vice versa.

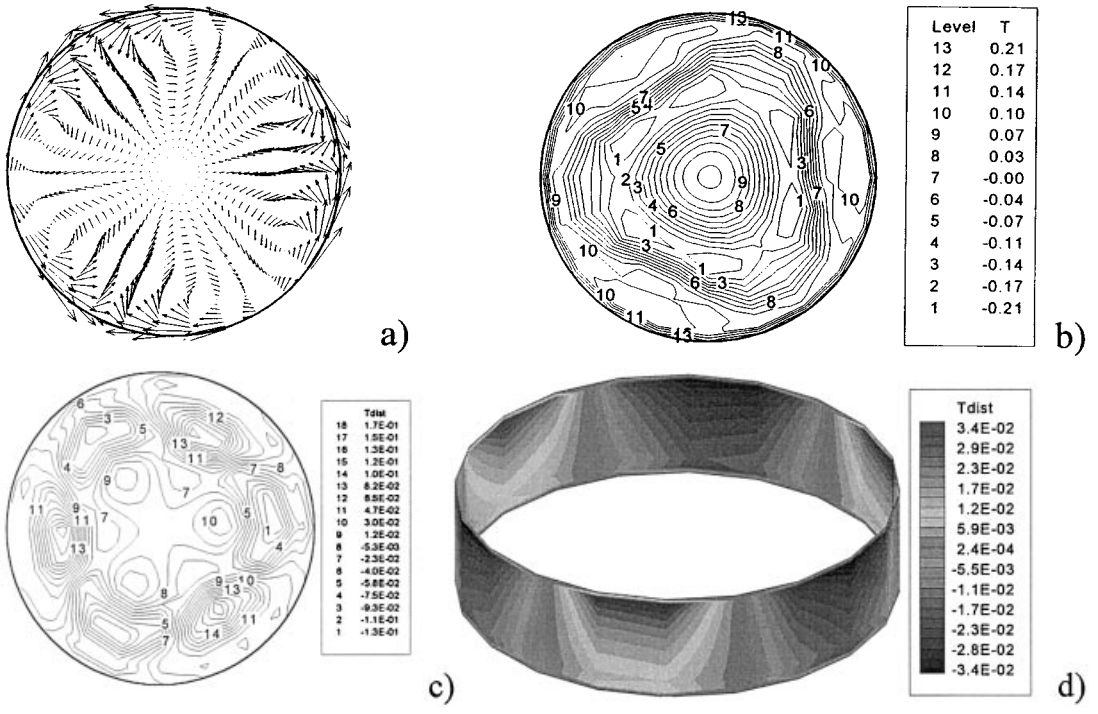

Figure 7. (a) Velocity field in the section $z = 0.5$ for $A = 0.25$; (b) temperature distribution and (c) temperature disturbances in the section $z = 0.75$ for $A = 0.25$; (d) temperature disturbance on the bridge surface for $A = 0.25$ ($Ma = 3.8 \times 10^4$).

For even critical wavenumbers, the flow field structure is on the whole three-dimensional and depends on the azimuthal co-ordinate, but in each axial plane the velocity and the temperature fields are symmetric and the time dependence is observed as a synchronous pulsation of the two symmetrical vortices.

The different behaviours of the velocity field in a meridian plane, depending on the critical wavenumber (even or odd) are shown in Figures 10–13 for two moments in time corresponding to the minimum and the maximum of the velocity oscillations during one cycle respectively.

For $A = 0.7$ ($m = 1$) one of the two vortex cells in the section prevails on the other one and is extended along the whole axial plane of the bridge; the other cell contracts and is confined in the hot corner. Moreover, since in the boundary layer near the cold disk steep axial gradients of temperature are present, here a small Marangoni cell is still present driven by the surface temperature distribution (see Figure 10). For $A = 0.5$ ($m = 2$) the velocity field in the section of Figure 11 is symmetric and the convective cells travel axially

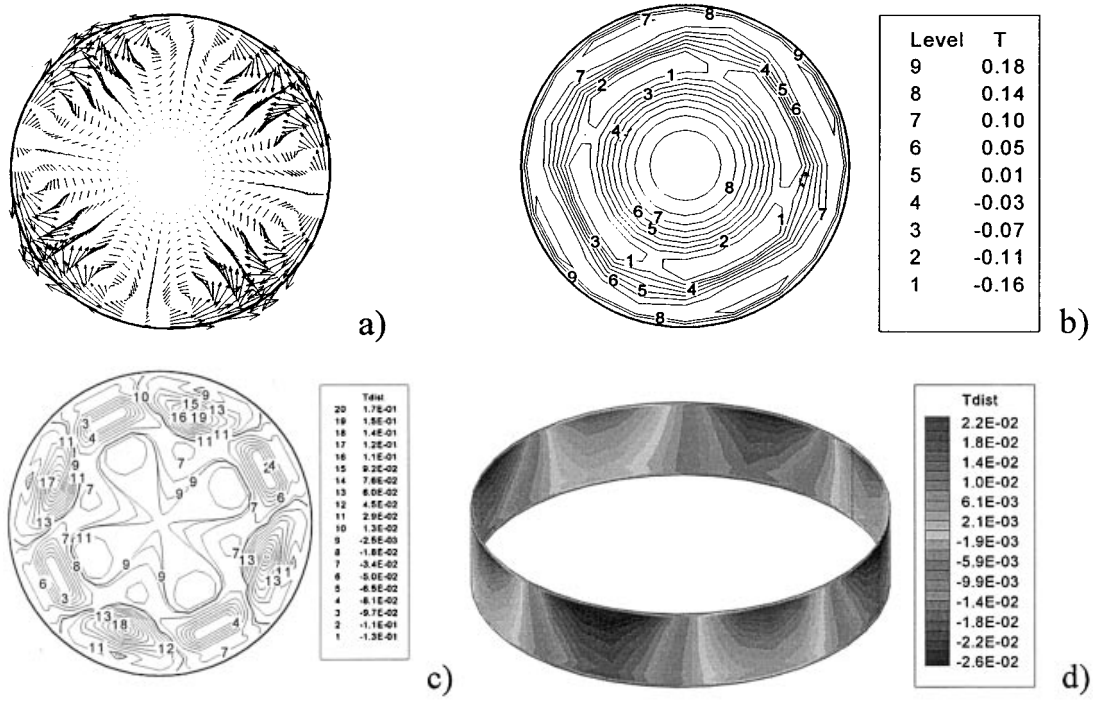

Figure 8. (a) Velocity field in the section $z = 0.5$, (b) temperature distribution and (c) temperature disturbances in the section $z = 0.75$ for $A = 0.2$ ($Ma = 3.9 \times 10^4$); (d) temperature disturbance on the bridge surface for $A = 0.2$ ($Ma = 3.9 \times 10^4$).

up and down. The situations for $A = 0.25$ ($m = 3$) and $A = 0.2$ ($m = 4$) are illustrated in Figures 12 and 13 respectively. The liquid bridge in this case is very short and the two driving cells are confined near the free surface, with other counter-rotating vortex cells induced by continuity in the interior of the bridge.

Similar results were obtained using two-dimensional computations by Rybicki and Floryan [24] who found, for short bridges, the emergence of several layers of vortices, with the strength of each layer decreasing approximately exponentially with the distance from the surface.

For $A = 0.5$ only one toroidal vortex exists (Figure 11). When A is reduced, small additional vortices located around the axis of rotation and attached to the side-walls emerge. These vortices are clearly visible in the bridges of aspect ratio 0.25 and 0.2. For $A = 0.25$ (Figure 12) the critical wavenumber is odd ($m = 3$) and the additional counter-rotating vortex cells in the interior of the bridge are attached one to the hot disk and the other to the cold disk; for $A = 0.2$ (Figure 13) they are symmetric, since the wavenumber is even ($m = 4$).

Table IV shows that, while the critical wavenumber changes with the aspect ratio, the critical Marangoni number does not change much and it is a smooth decreasing function of the aspect

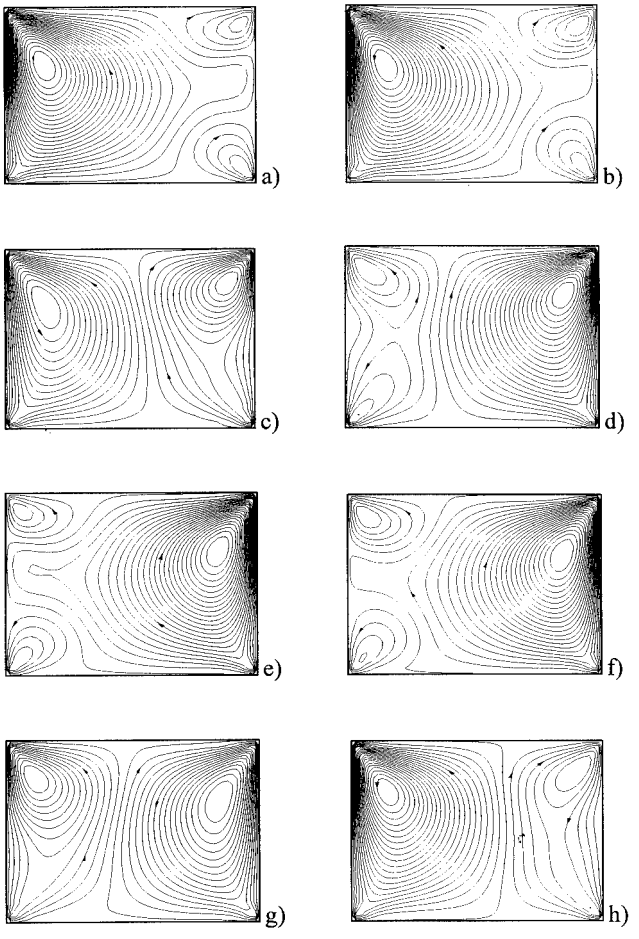

Figure 9. Streamlines of the projected velocity vectors on the meridian plane $\varphi = 0$ for $A = 0.7$ and $Ma = 3.35 \times 10^4$ (the field is shown in (a)–(h) corresponding to $t = 0$, $\tau/8$, $\tau/4$, $3\tau/8$, $\tau/2$, $5\tau/8$, $3\tau/4$, $7\tau/8$).

ratio of the bridge. This behaviour can be explained by the fact that when the aspect ratio decreases, the ratio of the free surface area S_l (where the 'driving force' is present) divided by the end walls area S_w (where 'no-slip' prevails), $S_l/S_w = 2A$ also decreases, increasing viscous effects and stabilizing the flow field.

On the other hand, the non-dimensional frequency of the oscillations ($f = f_c \cdot D^2/\alpha$, where f_c is the computed critical frequency) strongly increases (Table IV).

This behaviour can be explained considering that when the aspect ratio is reduced, the critical wavenumber increases, consequently minima and maxima of the azimuthal disturbances are closer to each other.

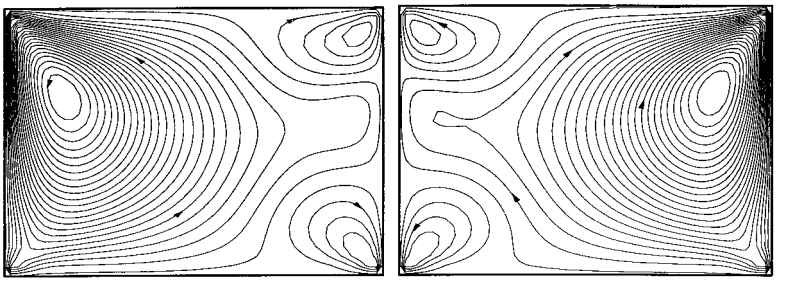

Figure 10. Streamlines of the projected velocity vectors on the meridian plane $\varphi = 0$ for $A = 0.7$ and $Ma = 3.35 \times 10^4$ (the field is shown in (a) and (b) corresponding to $t = 0$ and $t = \tau/2$).

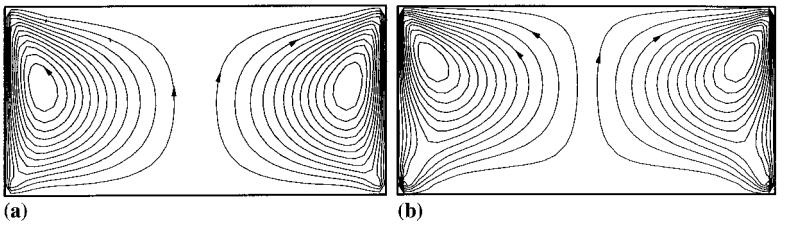

Figure 11. Streamlines of the projected velocity vectors on the meridian plane $\varphi = 0$ for $A = 0.5$ and $Ma = 3.5 \times 10^4$ (the field is shown in (a) and (b) corresponding to $t = 0$ and $t = \tau/2$).

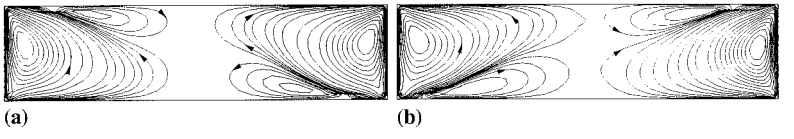

Figure 12. Streamlines of the projected velocity vectors on the meridian plane $\varphi = 0$ for $A = 0.25$ and $Ma = 3.8 \times 10^4$ (the field is shown in (a) and (b) corresponding to $t = 0$ and $t = \tau/2$).

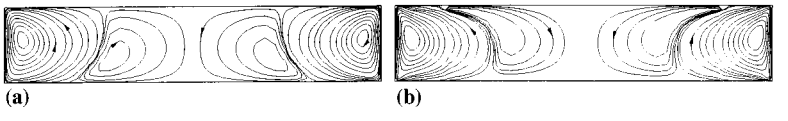

Figure 13. Streamlines of the projected velocity vectors on the meridian plane $\varphi = 0$ for $A = 0.2$ and $Ma = 3.9 \times 10^4$ (the field is shown in (a) and (b) corresponding to $t = 0$ and $t = \tau/2$).

4.2. Comparison with previous experimental and numerical results

The critical wavenumbers obtained for high-Prandtl number liquids and different aspect ratios in previous studies are summarized in Table V(a) and (b), which report, respectively, all the available experimental and numerical results. In the table the present numerical results are presented for comparison.

In particular (Table V(a)) Chun and West [1,2] found experimentally $m = 2$ mode for octadecane ($Pr = 25$) liquid bridge of small aspect ratio ($A = 0.45$) and $m = 1$ for $A > 0.5$. Preisser *et al.* [3] found for $NaNO_3$ zones ($Pr = 9.7$) $m = 1$ for $A > 0.65$, $m = 2$ for $0.4 < A < 0.65$, $m = 3$ for $0.25 < A < 0.4$, $m = 4$ for $A < 0.25$ and the empirical relation $2mA \cong 2.1$ between mode and aspect ratio, showing that the critical azimuthal wavenumber increases when the aspect ratio is reduced. For the same liquid, Velten *et al.* [4] found large ranges with modes $m = 2$, 3, 4 around $A = 0.55$, 0.375 and 0.3 respectively; the product $2mA$ was found to have a value of 2.25, which is almost the same as that of Preisser *et al.* [2].

In a KCl melt ($Pr = 1$), Velten *et al.* [4] found instabilities with the azimuthal component with $m = 2$ around $A = 0.6$, $m = 3$ around $A = 0.35$ and $m = 4$ around $A = 0.25$ and $2mA \cong 2.1$.

In liquid bridges of $C_{24}H_{50}$ ($Pr = 49$) Velten *et al.* [4] found $m = 2$ near $A = 0.45$, $m = 3$ near $A = 0.32$ and $m = 1$ (not observed in KCl and $NaNO_3$) near $A = 0.6$ and $2mA \cong 1.8$.

Muehlner *et al.* [8] found $m = 1$ for a liquid bridge of tetradecamethylhexasiloxane ($Pr = 35$) for $A = 0.5$. Table V(a) shows that the present numerical results are in qualitative agreement with the previous experimental findings available for different values of the Prandtl number. In particular, these results satisfy the correlation function $2mA \cong 1.6$ between the azimuthal wavenumber and the aspect ratio; the value 1.6 is almost the same as that obtained by Velten *et al.* [4] for $Pr = 49$.

Muehlner *et al.* [8] used an infrared thermocamera with wavelengths centred at 4.61 μm and observed, for a $Pr = 35$ and $A = 0.5$, oscillatory Marangoni convection at $Ma = 13000$ in the form of a travelling wave with $m = 1$ (in contrast to the present results, which give for $Pr = 30$ and $A = 0.5$, $m = 2$ and $Ma_c = 22000$). Concerning the apparent discrepancies between the experimental results reported by Muehlner *et al.* [8] and the present numerical results, a number of remarks can be pointed out.

Muehlner *et al.* [8] considered a non-cylindrical liquid bridge with a volume smaller than the volume of the cylinder with same diameter and length (0.065 cm^3, as reported in Reference [7], where the same experiment of Muehlner *et al.* [8] is described, in contrast to the cylindrical one 0.085 cm^3). In the present work, a cylindrical zone has been investigated. This may explain the different results since, as is well known and recognized by the same authors [8], the critical conditions for the onset of time dependence are sensitive to the volume. In fact, as shown by Chen and Hu [18], a 20 per cent change in volume can give rise to a 100 per cent change in the critical Marangoni number. In addition, the present calculations show that the transition from $m = 2$ to $m = 1$ as the most unstable azimuthal wavenumber occurs for $A \cong 0.52$ and this together with the different shape of the bridge could explain the different azimuthal wavenumbers.

Table V(b) summarizes the previous numerical results. In particular Rupp *et al.* [10] found $m = 2$ for $A = 0.6$ and for $Pr = 49$, but unfortunately they did not make a study on the

Table V. Critical azimuthal wavenumber versus the Prandtl number and versus the geometrical aspect ratio; comparison between the present numerical results and other (a) available experimental results and (b) available numerical and theoretical results.

(a)

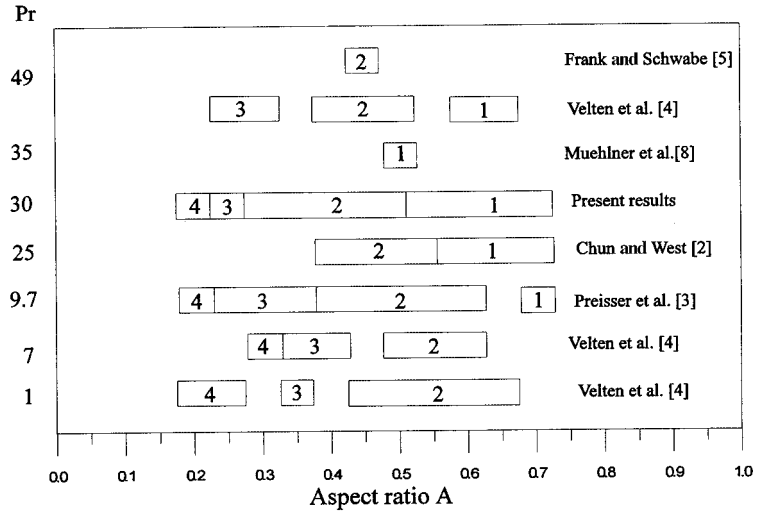

(b)

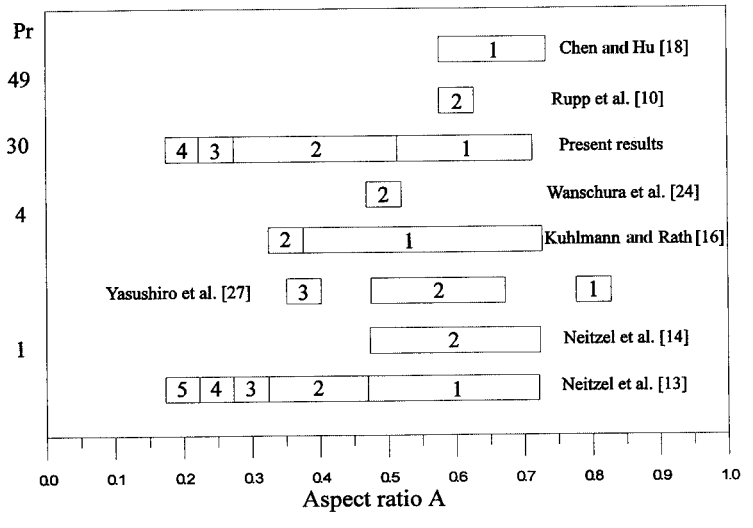

influence of the geometrical aspect ratio (A). Monti *et al.* [20,21] found $m = 1$ for $A = 1$ and $Pr = 30$ and 74.

Xu and Davis [11] used linear stability theory to determine sufficient conditions for instability to infinitesimal disturbances for a half zone of infinite aspect ratio. They found that there is a critical value Pr^* (50) of the Prandtl number such that if $Pr < Pr^*$, the mode $m = 1$ is preferred, while if $Pr > Pr^*$ the mode $m = 0$ is preferred. However, since they considered liquid bridges of infinite length, their results cannot be directly applied to a finite-length liquid bridge.

Using energy stability theory, Neitzel *et al.* [13] found for a fluid of $Pr = 1$ a monotonic cascade from $m = 5$ to $m = 1$ over the range $0.2 < A < 0.5$, with $m = 1$ persisting to $A = 0.9$.

Recently, Yasushiro et al. [28], using three-dimensional computations, have found for $Pr = 1$, $m = 1$, 2, 2 and 3 for $A = 0.8$, 0.65, 0.5 and 0.375 respectively.

In the linear stability results of Neitzel *et al.* [14], for all cases considered ($Pr = 1$ and $0.5 < A < 0.7$), the minimizing azimuthal wavenumber was $m = 2$. These results agree with those obtained by Chen and Roux [17] who found for a large range of Prandtl numbers and aspect ratios, $m = 2$ as the most critical wavenumber. These findings, however, do not agree with the results obtained in this work, which show a dependence between the critical mode number m and the aspect ratio, according to the experimental observation by several investigators.

Chen and Hu [18], using linear instability analysis, analysed the influences of the aspect ratio ($0.6 \leq A \leq 1.4$) and of the liquid bridge volume on the critical Marangoni number. They found $m = 1$ as the most critical wavenumber for all the aspect ratios investigated and for $Pr = 1$, 10 and 50 in agreement with the present results.

Kuhlmann and Rath [16] performed a linear stability analysis over a large range of Prandtl numbers. They found that for $A = 0.5$ and $1 < Pr < 30$ the most dangerous disturbances have wavenumber $m = 1$. However, there was some error in the calculations of Kuhlmann and Rath, which was discovered after the publication of their paper. In a more recent work (Wanschura *et al.* [25]), this error has been eliminated; for $0.8 < Pr < 5$ they found $m = 2$ for $A = 0.5$. The same value was found for $A = 0.5$ by Neitzel *et al.* [14] for $Pr = 1$, and $A = 0.5$, and in the present work for $Pr = 30$.

4.3. Analysis of the oscillatory model: standing waves and travelling waves

The numerical results obtained in this work show that, for all the aspect ratios considered, the flow immediately after the onset may be properly described by the dynamic model of an 'azimuthally standing wave'. The three-dimensional temperature disturbance consists of a number m of couples of disturbances (hot and cold) 'pulsating' at the same azimuthal positions along the interface and in the bulk (minimum and maximum disturbances at fixed azimuthal positions). These spots are responsible for thermocapillary effects in the azimuthal direction, causing $2m$ counter-rotating vortex cells in the transversal section.

After a second transition the instability mechanism becomes dominated by a travelling wave and the temperature spots rotate around the axis of the floating zone (the number of the spots depending on the aspect ratio as for the standing wave).

Figures 14 and 15 show the temperature and the vector plots in a transversal cross-section for the standing wave regime and $m = 2$ ($A = 0.4$, $Ma = 3.6 \times 10^4$). The pulsating temperature spots on the surface of the bridge are shown in Figure 16 (the period τ has been divided into four parts and the fields are shown in (a)–(d) corresponding to $t = 0$, $\tau/4$, $\tau/2$, $3\tau/4$). These temperature spots 'pulsate', i.e. the two cold spots grow in the axial direction during the shrinking of the two hot spots and vice versa, but the azimuthal positions of these extrema do not change. According to this behaviour, the convective cells in Figure 15 change periodically their sense of rotation. Their intensity is not constant in time; if the considered convective cell is clockwise oriented during the first half period, then during the second half of the period it vanishes and then reappears in the same azimuthal position anti-clockwise oriented (Figure 15). The behaviour of the surface spots is also directly related to the motion of the toroidal vortex centreline. As explained in Section 4.1, the position of the vortex centreline describes in the space a sine curve having two maxima and two minima in the z-direction (in the case $m = 2$). During half period, the maxima travel in the z-direction towards the cold disk and the minima travel in the z-direction towards the hot disk; in the second half the minima become maxima and vice versa.

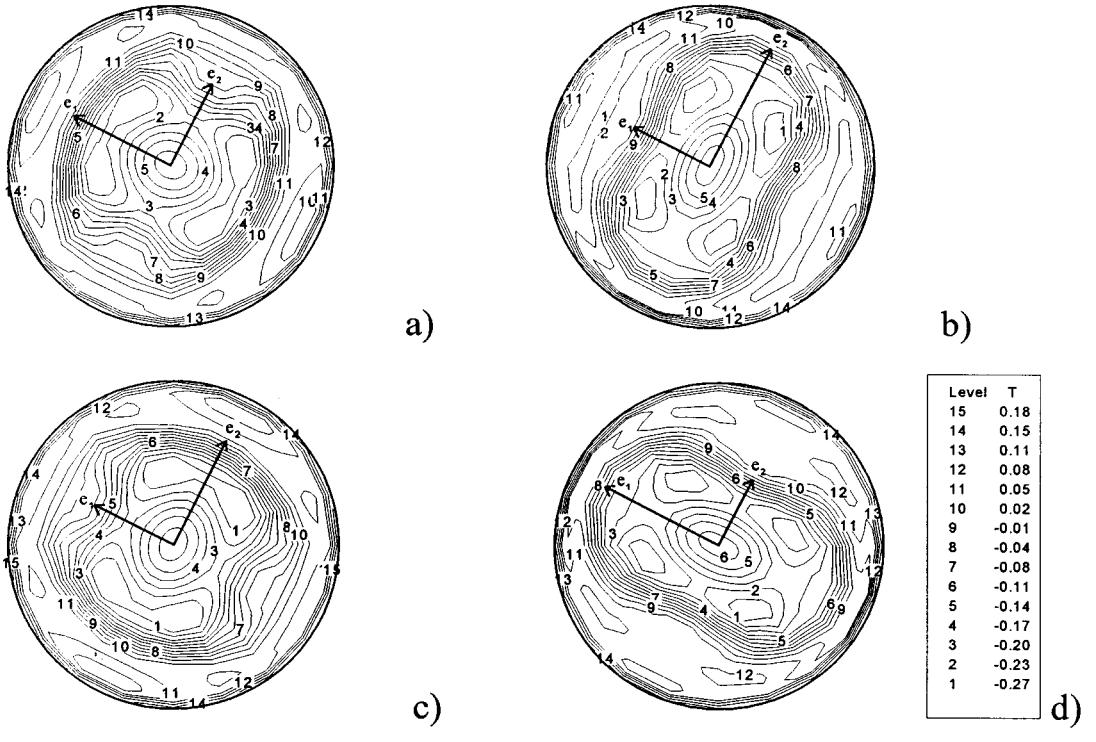

Figure 14. Temperature distribution in the section $z = 0.75$ for $A = 0.4$ and standing wave regime ($Ma = 3.6 \times 10^4$) (the field is shown in (a)–(d) corresponding to $t = 0$, $\tau/4$, $\tau/2$, $3\tau/4$).

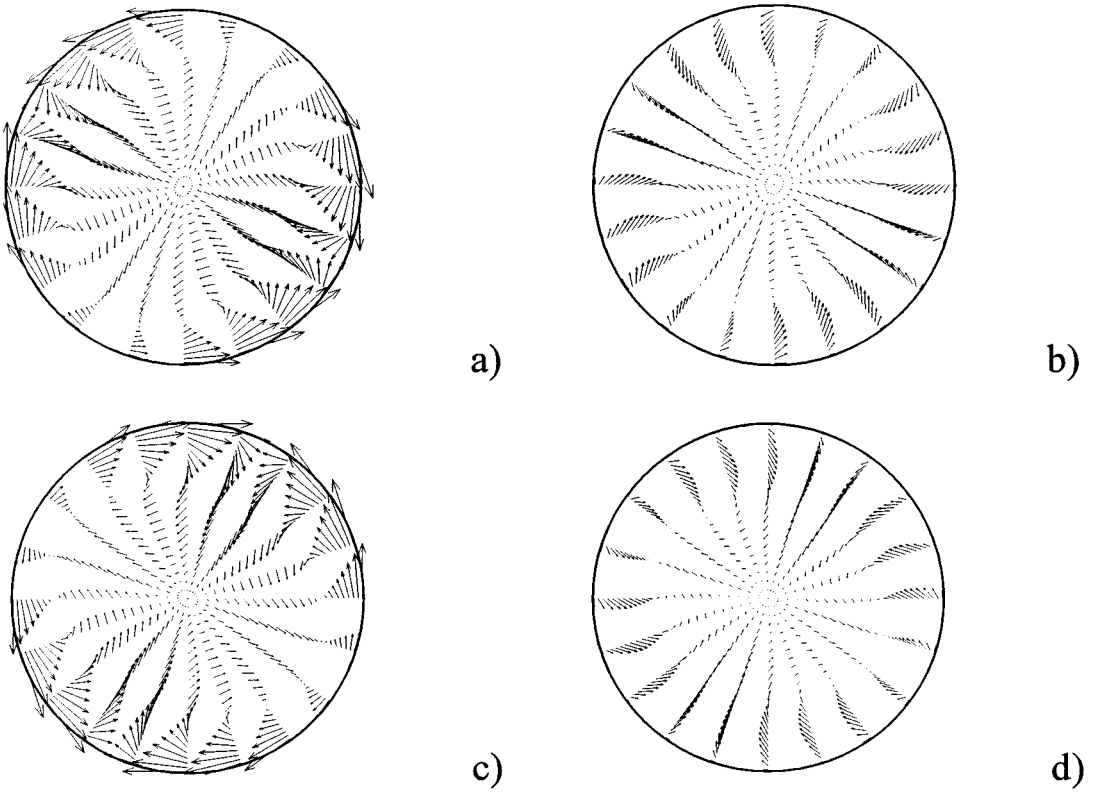

Figure 15. Velocity field in the section $z = 0.5$ for $A = 0.4$ ($Ma = 3.6 \times 10^4$) and standing wave regime (the field is shown in (a)–(d) corresponding to $t = 0$, $\tau/4$, $\tau/2$, $3\tau/4$).

Since the displacement up and down of the toroidal convection roll is coupled to displacement out and in, respectively, with respect to the axis of symmetry of the zone, this gives rise to an alternate expansion and contraction of the axes e_1 and e_2 of the elliptic inner region of the temperature field (Figure 14). One complete period for this time-dependent behaviour takes a time $1/f$, where f is the characteristic frequency of the oscillations.

Figures 17–19 show the thermofluid dynamic after the second transition to an azimuthally travelling wave. It can be observed that many differences exist with respect to the case of standing wave regime. In this case the behaviour is not 'pulsating', but rotating.

The surface temperature spots do not change their intensity and rotate around the perimeter of the liquid bridge. The vortex cells in the section orthogonal to the axis do not change their sense of rotation and their strength is constant in time (the cells never vanish, see Figure 18). The time-dependent behaviour of the velocity field is simply characterized by a full rotation of the entire flow pattern in the azimuthal direction. For the temperature field (Figure 17) it can be observed that the amplitude of the axes e_1 and e_2 is fixed, whereas the inner elliptic region

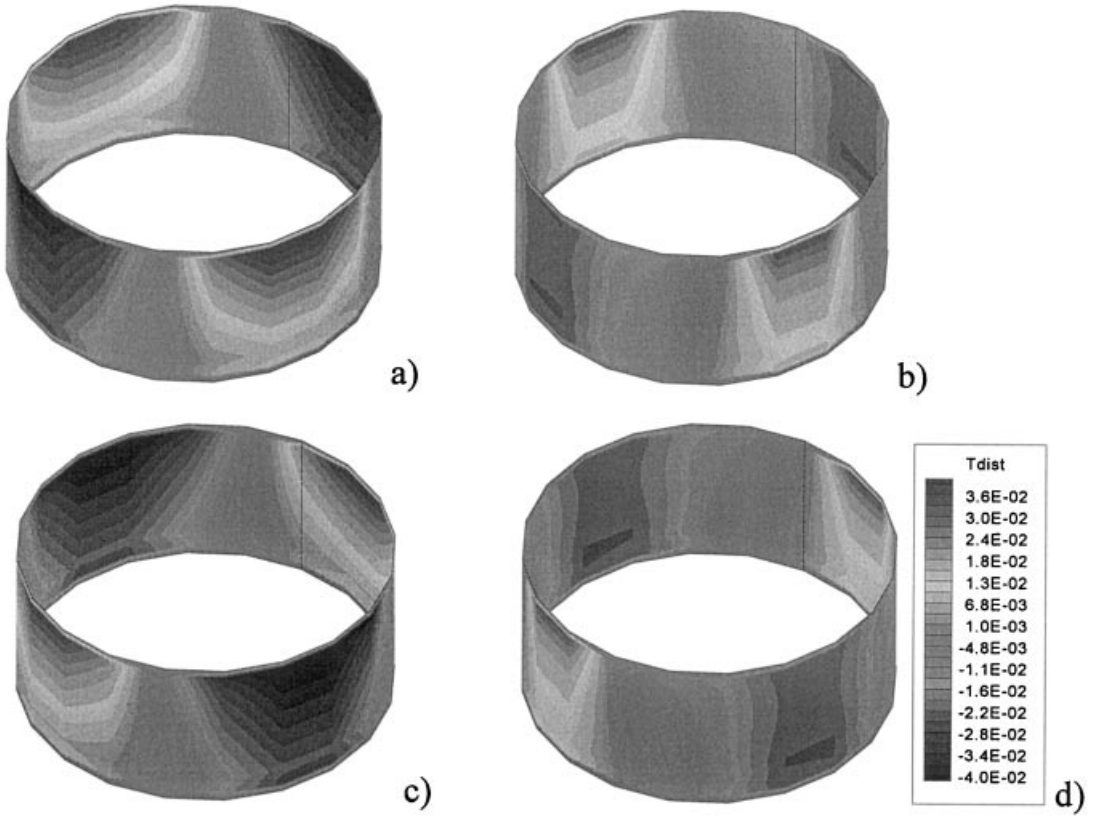

Figure 16. Temperature disturbance on the bridge surface for $A = 0.4$ ($Ma = 3.6 \times 10^4$) and standing wave regime (the field is shown in (a)–(d) corresponding to $t = 0$, $\tau/4$, $\tau/2$, $3\tau/4$).

rotates with the centre of rotation corresponding to the axis of symmetry. In this case one entire rotation of the configuration needs a time $2/f$.

The standing wave regime for $A = 0.25$ ($m = 3$) and for $A = 0.2$ ($m = 4$) are depicted in Figures 20 and 21 and Figures 22 and 23 respectively. In this case, the behaviour is similar to that described for the case $m = 2$, the only difference being the different number of spots and vortex cells in the azimuthal direction (Figures 20 and 22 show a pulsation of the inner triangle and quadrangle respectively: the nodes of these polygons are replaced in time by the presence of sides and vice versa). One complete period for this time-dependent behaviour takes a time of $1/f$ as in the case $m = 2$.

The rotating regime for these cases (not shown) is merely characterized by a full rotation of the thermofluid dynamic field as for $m = 2$ and the entire rotation of the configuration needs a time of m/f.

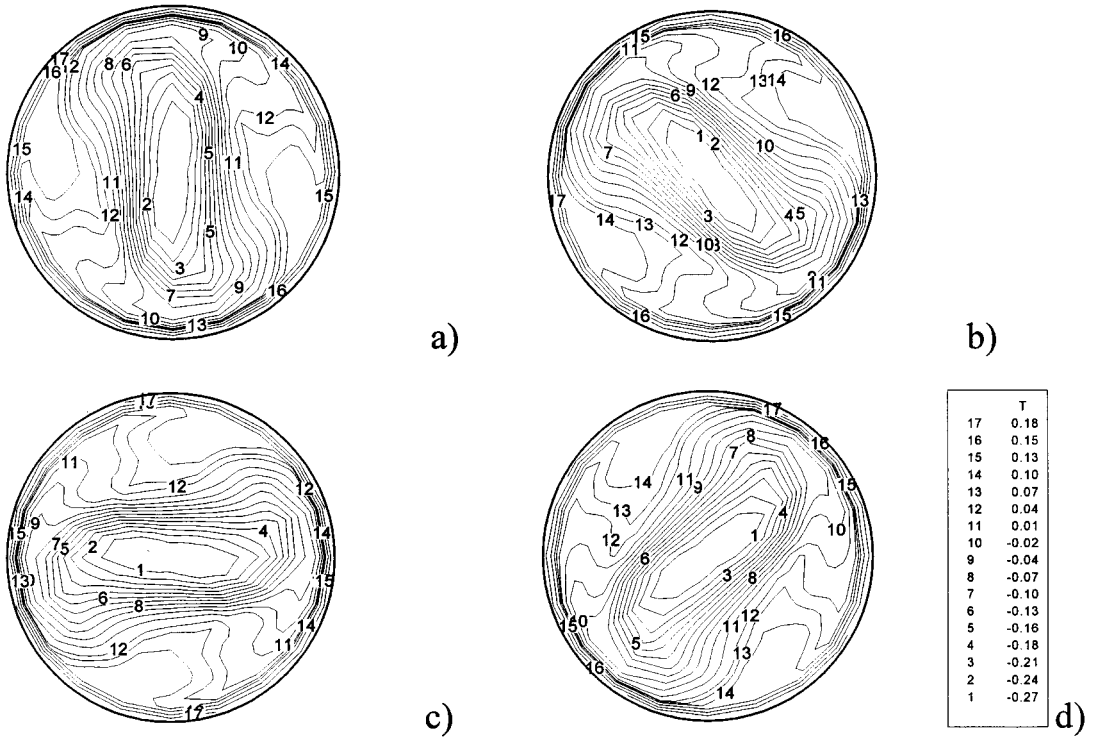

Figure 17. Temperature distribution in the section $z = 0.75$ for $A = 0.4$ ($Ma = 3.6 \times 10^4$) and travelling wave regime (the field is shown in (a)–(d) corresponding to $t = 0$, $\tau/4$, $\tau/2$, $3\tau/4$).

Although an azimuthally standing wave that develops in an azimuthally travelling wave after a certain time was observed for all the aspect ratios investigated, the standing wave model was found to be more stable for small aspect ratios. For $0.2 < A < 0.3$, the standing wave regime lasts for a long time, whereas for $A > 0.3$, the transition from the pulsating regime to the rotating regime occurs after a short transition time.

It must be emphasized that the azimuthal wavenumber and the fundamental frequency are independent of the type of oscillation (pulsating or rotating), so that it is not possible to identify the transition from one regime to the other using these values. However, another factor that can be considered a distinguishing mark between standing and travelling waves is the behaviour of the average Nusselt number on the cold and hot disks of the bridge.

The computations show that during the standing wave regime these average values are not constant in time but oscillate at a frequency that is double with respect to the frequency of the temperature oscillations.

When the standing wave regime develops in a travelling wave regime the average Nusselt number on both plates converges to a constant value which is smaller than the average Nu value related to the axisymmetric regime.

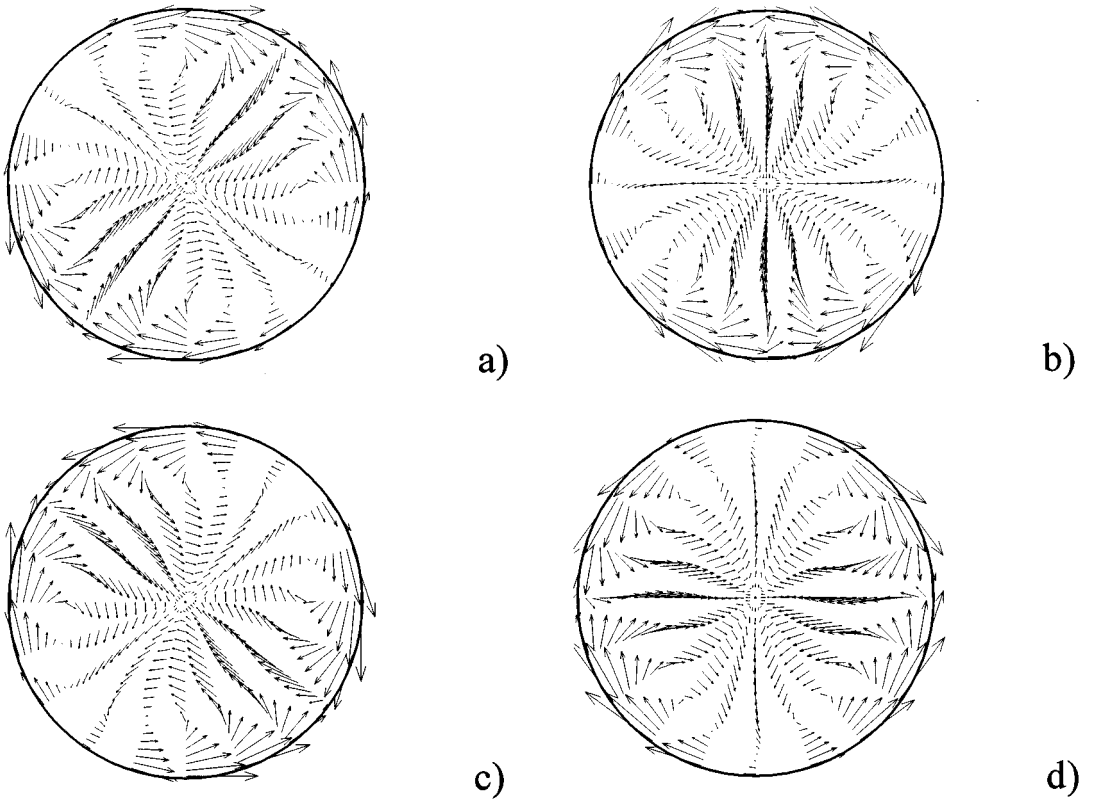

Figure 18. Velocity field in the section $z = 0.5$ for $A = 0.4$ ($Ma = 3.6 \times 10^4$) and travelling wave regime (the field is shown in (a)–(d) corresponding to $t = 0,\ \tau/4,\ \tau/2,\ 3\tau/4$).

This is shown in Figure 24(a). The Nusselt number oscillates with a frequency $2f$ during the pulsating regime but the amplitude of the oscillations decreases in time up to a constant value when the standing wave develops in travelling wave.

The decrease of the average Nusselt number can be explained on the basis of the amount of axial momentum that is converted in azimuthal momentum after the onset. The azimuthal momentum, in fact, does not contribute to the axial heat transfer near the disks.

Moreover, in the present computations it has been found that the standing waves have not a detectable azimuthal mean flow (i.e. the mean value of the oscillating azimuthal velocity is zero).

The present results have shown that during the standing wave regime, the whole body of liquid bridge does not rotate (i.e. the azimuthal disturbance does not carry on its motion). In the travelling wave regime, instead, a small azimuthal mean flow has been observed (see the (b)s of Figures 4 and 24, where at a certain distance from the onset, when the instability

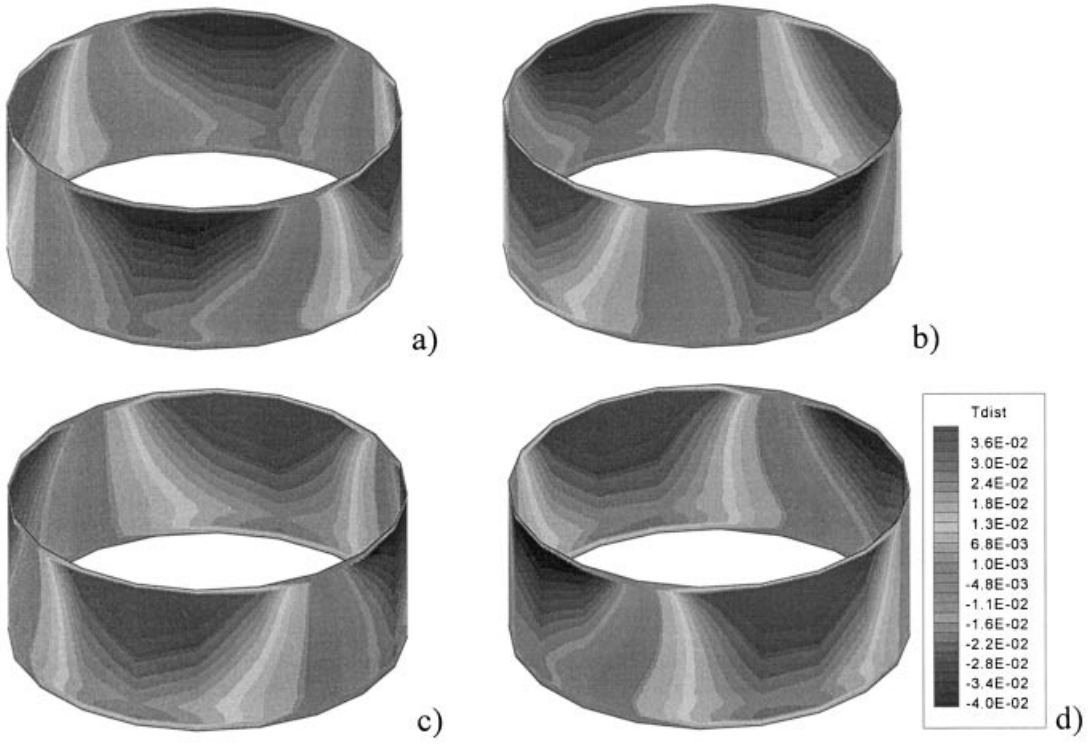

Figure 19. Temperature disturbance on the bridge surface for $A = 0.4$ ($Ma = 3.6 \times 10^4$) and travelling wave regime (the field is shown in (a)–(d) corresponding to $t = 0$, $\tau/4$, $\tau/2$, $3\tau/4$).

mechanism becomes dominated by a travelling wave regime, the velocity profile loses its symmetry with respect to the zero value). This azimuthal mean flow, however, has been found to be very small (in Figure 24(b) for $Pr = 4$ and $A = 0.5$, the mean value of the azimuthal velocity is 10 per cent of the amplitude, whereas in Figure 4(b) for $Pr = 30$ and $A = 0.5$, the mean value is 3 per cent of the amplitude).

This is in agreement with the findings of Schwabe *et al.* [9], who under supercritical conditions found an additional clearly visible oscillation in the azimuthal direction. It was found that the azimuthal oscillation of tracer particles captured in the vortex centre was not symmetrical and characterized by a mean value of the azimuthal velocity (i.e. net flow in the azimuthal direction). They observed groups of tracer particles that were trapped in the centre of the Marangoni vortex roll, moving azimuthally back and forth asymetrically, such that there was a net movement of the particles in the direction of propagation of the travelling wave.

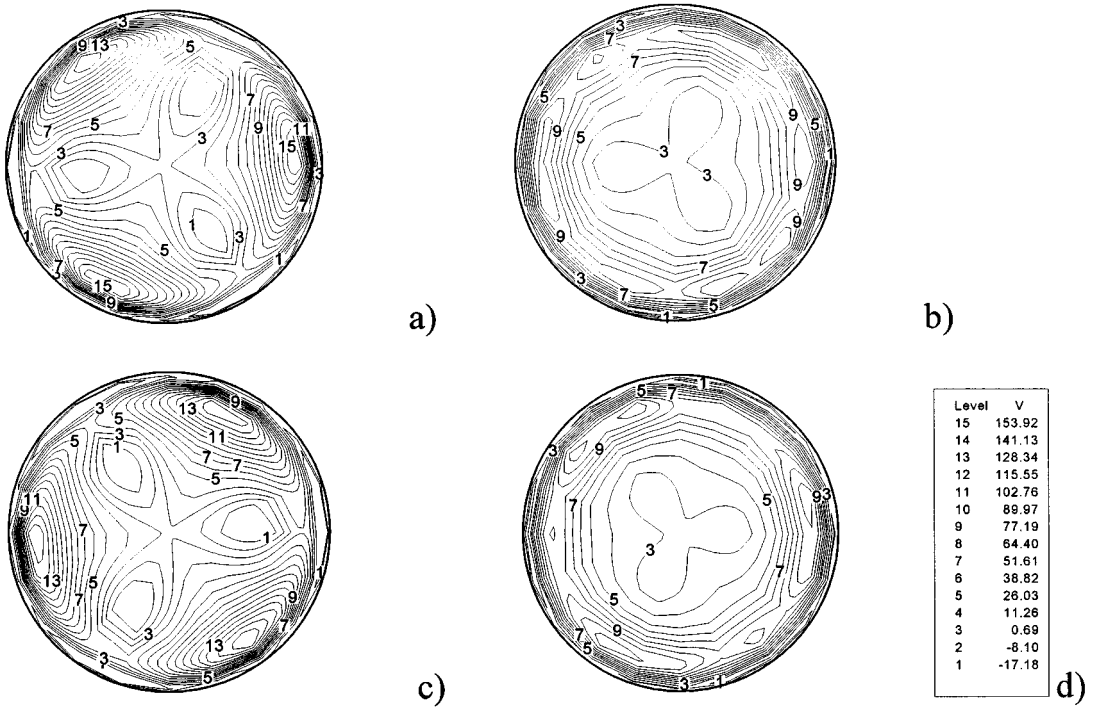

Figure 20. Radial velocity distribution in the section $z = 0.75$ for $A = 0.25$ ($Ma = 3.8 \times 10^4$) and standing wave regime (the field is shown in (a)–(d) corresponding to $t = 0$, $\tau/4$, $\tau/2$, $3\tau/4$).

4.3.1. Discussion. The computed spatio-temporal structures of the three-dimensional oscillatory Marangoni convection discussed above agree with those predicted by the previous linear stability analyses, according to which, for large Pr, the basic Marangoni flow loses its stability due to a pair of counter-propagating azimuthal waves, with a phase depending not only on φ and t but also on the radial and axial co-ordinates r and z.

The wave front F of such hydrothermal waves is inclined with respect to z. Since the constant phase surfaces can be imagined as vertical planes that have been twisted around the vertical axis, the twist being given by a phase $G(r, z)$, each wave having an amplitude $A(r, z)$ can be represented according to Kuhlmann and Rath [26] as

$$F_{\pm} = A(r, z) \exp\{\mathrm{i}[\pm m\varphi - \omega t + G(r, z)]\} \tag{10}$$

A superposition of two counter-propagating waves with the same amplitude results in

$$F = 2A(r, z) \cos(m\varphi) \cos(\omega t - G(r, z)) \tag{11a}$$

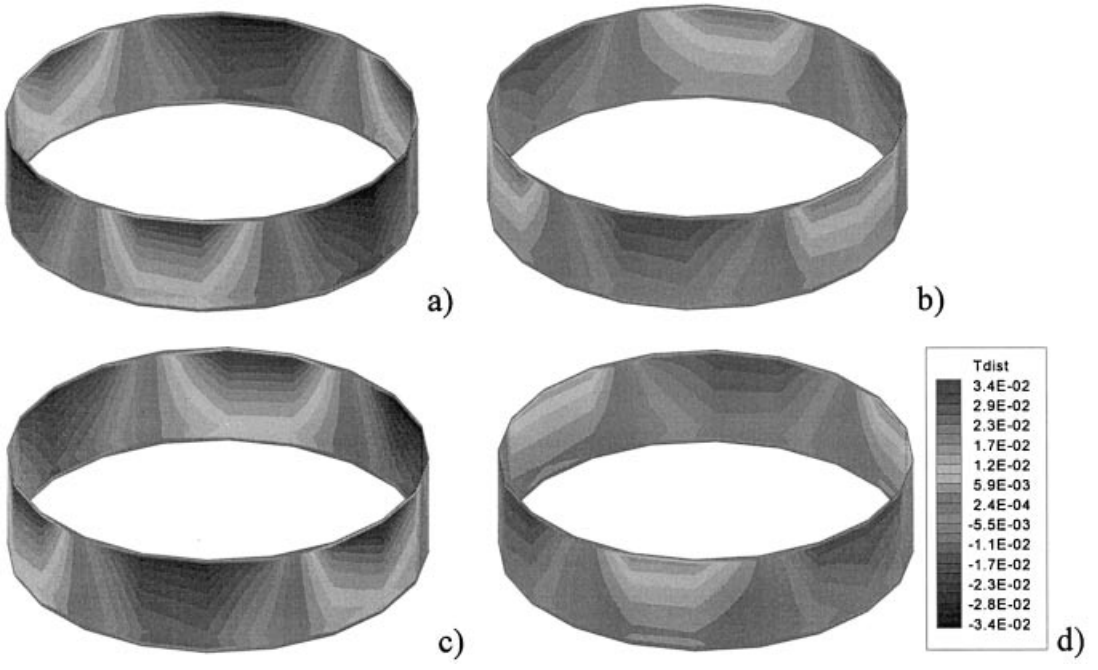

Figure 21. Temperature disturbances on the bridge surface for $A = 0.25$ ($Ma = 3.8 \times 10^4$) and standing wave regime (the field is shown in (a)–(d) corresponding to $t = 0,\ \tau/4,\ \tau/2,\ 3\tau/4$).

Since in this case the oscillatory term does not depend on φ, maximum and minimum disturbances are fixed in space and the minimum is continually replaced by the maximum and vice versa as soon as $\cos(\omega t - G(r, z))$ changes its sign. These extrema in the disturbance distribution give rise to hotter and colder zone in the bridge and the three-dimensional temperature disturbance consists of a number m of couples of spots (hot and cold) pulsating at the same azimuthal positions along the interface.

When the amplitude of the two hydrothermal waves is not the same, the superposition gives

$$F \cong A(r, z)a(m\varphi)\cos[b(m\varphi, G) - \omega t] \tag{11b}$$

(the functions a and b are reported on in Reference [26]) so that the oscillatory term depends on φ; in this case the minimum and maximum disturbances travel in the azimuthal direction and the phase of the oscillations depends continuously on φ.

When the oscillations are measured in points with the same axial and radial co-ordinates but at different azimuthal positions, for the standing wave only two values of the azimuthal phase shift are allowed ($\Delta\phi = 0$ if the points are placed on the same spot, $\Delta\phi = \pi$ if the two points belong to two different spots); on the contrary, for the travelling wave the possible values of the phases are not discrete.

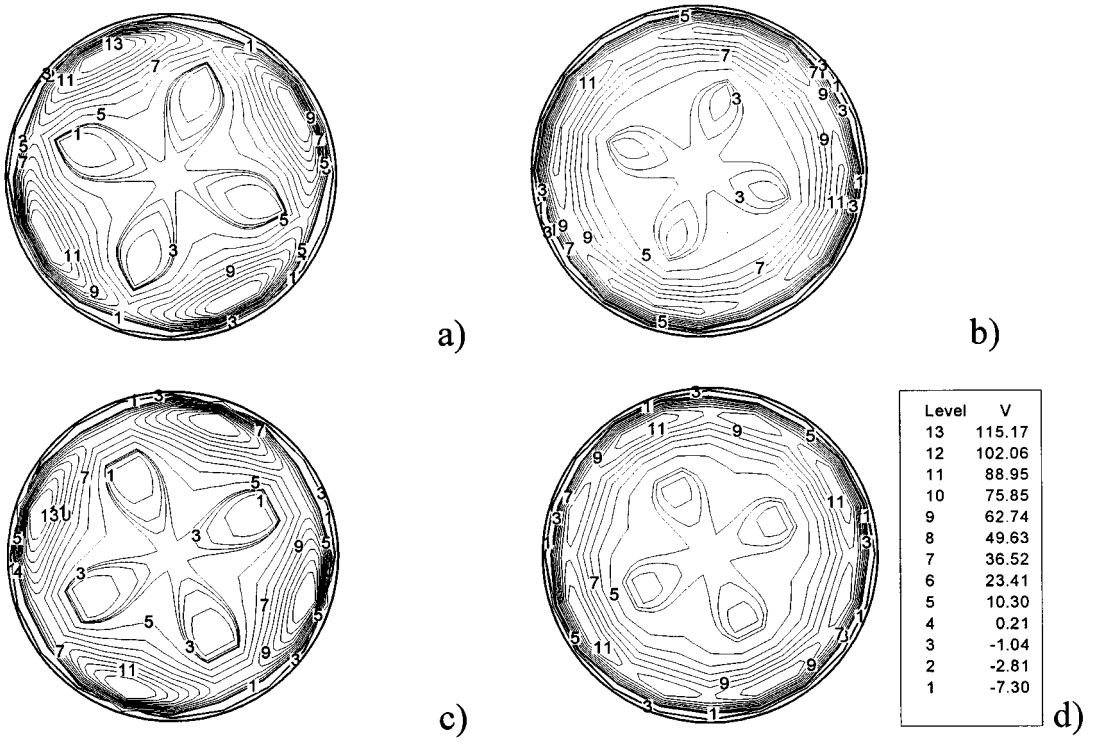

Figure 22. Radial velocity distribution in the section $z = 0.75$ for $A = 0.2$ ($Ma = 3.9 \times 10^4$) and standing wave regime (the field is shown in (a)–(d) corresponding to $t = 0$, $\tau/4$, $\tau/2$, $3\tau/4$).

The linear stability theory cannot predict if the standing wave or the travelling wave instability prevails since the relative amplitude of the two counter-propagating azimuthal waves depends on non-linear effects; the present computations that are based on the solution of the complete and non-linear Navier–Stokes equations show that the travelling wave model appears after the standing wave regime (after a time dependent on the aspect ratio of the liquid bridge). Probably this behaviour can be explained by the fact that at the beginning two counter-propagating waves with equal amplitude are formed, while in a second phase one of these waves prevails over the other.

The azimuthally travelling wave has been observed by different investigators, either on ground or in microgravity [1–6,8,9].

Schwabe *et al.* [9] used a stereo microscope (rather than a light cut technique) and observed in the bulk fluid dark inclined stripes moving in horizontal direction from one side of the floating zone to the other. These stripes (moving horizontally) were interpreted as a direct manifestation of azimuthally travelling thermal waves, since they were generated by densely packed tracer particles bunched in a line wound around the toroidal convection roll moving azimuthally.

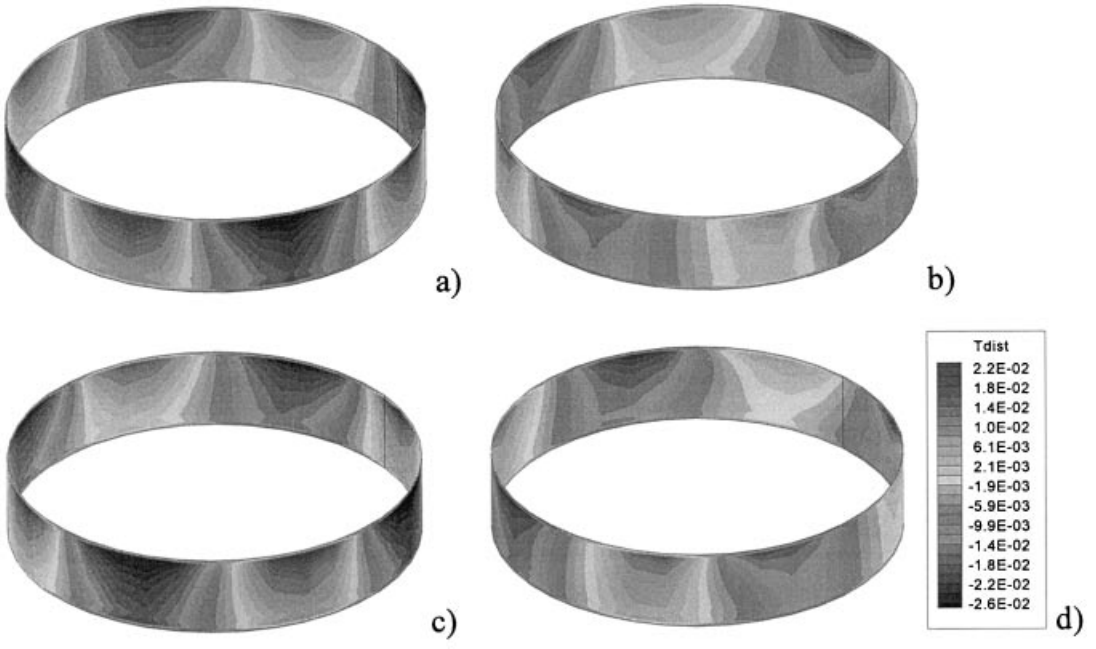

Figure 23. Temperature disturbances on the bridge surface for $A = 0.2$ ($Ma = 3.9 \times 10^4$) and standing wave regime (the field is shown in (a)–(d) corresponding to $t = 0$, $\tau/4$, $\tau/2$, $3\tau/4$).

Velten *et al.* [4], measuring the temperature near the free surface by three thermocouples positioned at the same radial co-ordinate but at different azimuthal positions, observed two different non-axisymmetric spatial structures of Marangoni convection: (1) running waves with an azimuthal component (corresponding to the travelling wave regime observed by other investigators); (2) axially running waves with deformed wave front. The latter regime corresponds to the standing wave regime, as demonstrated by Kuhlmann and Rath [26].

Recently, Frank *et al.* [5] using a light cut technique observed clearly pulsating and rotating regimes.

In the present paper the criterion to detect the regime (pulsating or rotating) has been based on the phase shift between two 'numerical' probes located on the free surface at the same axial position with an angular shift of $90/m°$. As discussed in Section 4.1, each surface spot has an angular extension of $360/2m°$. During the standing wave regime two cases are possible: (1) the two thermocouples are located on the same spot (the phase shift is 0); (2) the two probes are located on two adjacent different spots (the phase shift is π). When the regime is rotating the two probes give signals that show a constant phase shift related to the angular distance between them (for an angular shift of $90/m°$ the phase shift is $\pi/2$).

According to the discussion above, two numerical probes having an angular shift of $90/m°$ measure a phase shift of 0 or π during the standing wave regime. In the travelling wave regime,

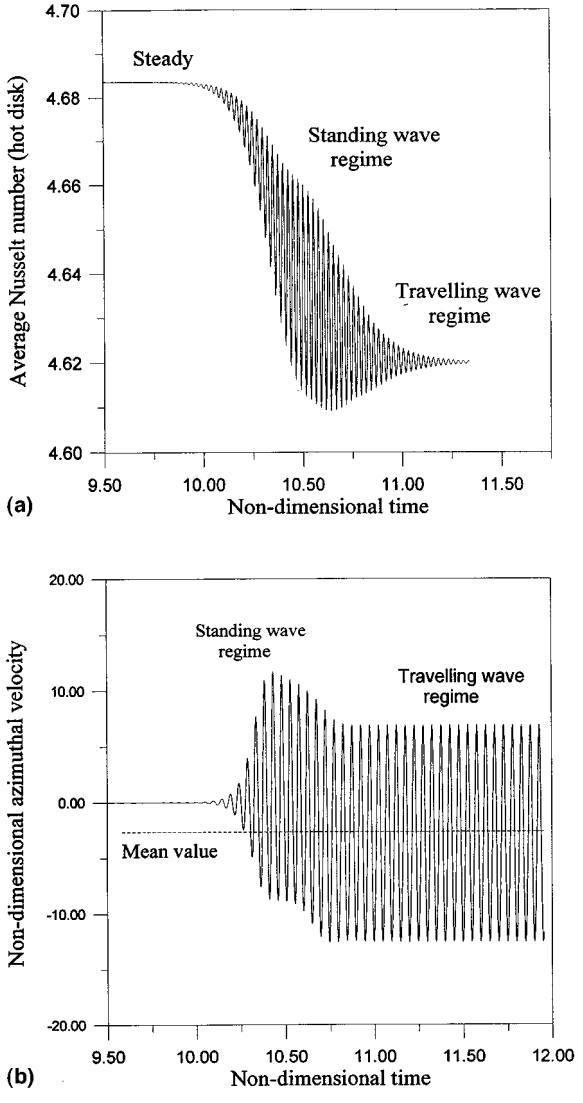

Figure 24. (a) Average Nusselt number on the hot disk versus time in the case $A = 0.5$, $Pr = 4$, $Ma = 4800$; (b) azimuthal velocity in the point $z = 0.75$, $r = 0.5$, $\varphi = 0$ for $A = 0.5$, $Pr = 4$, $Ma = 4800$.

the same probes measure instead a phase shift of $\pi/2$. Monitoring this phase shift it is possible to detect the regime and in particular the transition from one to the other.

Between these two regimes an intermediate (pulso-rotating) regime occurs, with a phase shift increasing with time from zero (or π) up to $\pi/2$ (during this transient time, the phase shift corresponds to values of the azimuthal wavenumber that are not integer); in the present paper the transition time is defined as the time corresponding to a 'pure' rotating regime ($\Delta\phi = \pi/2$).

4.4. Disturbances propagation velocity

This section will be dedicated to the discussion of the results obtained for the different aspect ratios considered in the numerical analysis, on the basis of the concept of the azimuthal velocity of propagation of the disturbances and of previous experimental results reported in the literature.

As discussed before, the transition from the standing wave regime to the travelling wave occurs after a short transition time if the aspect ratio is high, whereas it is quite stable and prevails for a long time if the aspect ratio is low (see Figure 25).

This behaviour can be explained by the velocity of propagation of the hydrothermal disturbances in the liquid, since this velocity is a function of the aspect ratio and of the Marangoni number. In particular, the propagation speed of the travelling disturbances is defined as

$$\tilde{V}_p = \frac{2\pi R}{m\tau} \tag{12}$$

where R is the radius of the bridge, m is the critical mode number and τ the period of the oscillations. This velocity in non-dimensional form (see Table IV) reads

$$V_p = \tilde{V}_p \frac{D}{\alpha} = \frac{2\pi R}{m\tau^* D^2/\alpha} \frac{D}{\alpha} = \frac{\pi}{m} f \tag{13}$$

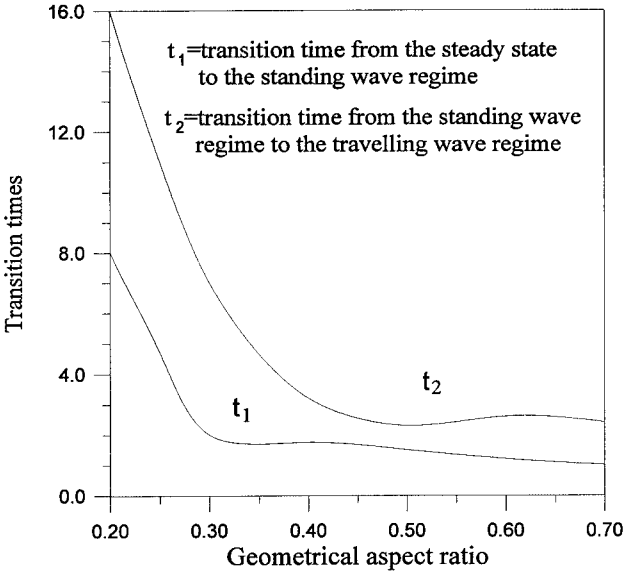

Figure 25. Transition times versus the geometrical aspect ratio ($Ma = 1.5Ma_c$).

where τ^* and f are the dimensionless period and the dimensionless frequency of the oscillations respectively. The propagation speed of the temperature disturbances is determined by the relative importance of the two contributions to the overall heat transfer (conduction and convection).

Hence, it follows that the travelling speed of the azimuthal perturbation is proportional to the Marangoni number as pointed out by Chun and West [1].

In Reference [27] it has been found experimentally that the dimensionless frequency can be expressed as

$$f = k\frac{1}{2\pi}\alpha Ma^{2/3}L^{-3/2}D^{-1/2}\frac{D^2}{\alpha} = k\frac{1}{2\pi}Ma^{2/3}A^{-3/2} \tag{14}$$

where k depends on the Prandt number of the liquid: $k \cong 0.7$ for $Pr = 30$ and substituting Equation (14) into Equation (13), it follows that

$$V_p \propto \frac{1}{2mA}Ma^{2/3}A^{-1/2} \tag{15}$$

Since all the liquid bridges are made with the same silicone oil ($Pr = 30$, $\alpha = 6.5 \times 10^{-8}$ $m^2\,s^{-1}$), since $2mA$ is almost constant ($2mA = 1.6$) and since Ma_c does not change much with decreasing the aspect ratio, it is clear that the disturbance propagation speed increases with $A^{-1/2}$ when A is reduced.

From Table IV (V_p computed using Equation (13)), it can be observed that the increase of the propagation speed of the travelling disturbances takes place mainly for $0.3 < A < 0.4$.

The results discussed before have shown that the standing wave regime is more stable and that it lasts for a long time if the aspect ratio is lower than 0.3–0.4.

Chun and West [1] observed that the time evolution of the flow after the onset should be related to the growth and propagation of the temperature disturbances. According to their theory, the growth or the damping of a small temperature disturbance depends on the ratio of the rapidity of the heat transfers by conduction and by convection. For the extreme case of very high conductive heat transfer, a temperature disturbance should die diffusing very rapidly in all directions. On the other extreme case of very high convective heat transfer, the disturbances should move with the flow, 'frozen' in the flow motion. Between these two extremas, the temperature disturbances that travel in different azimuthal directions with their own propagation velocity should interfere with each other and be amplified in the progress of time.

According to Chun and West [1] the velocity of propagation of the disturbances is a 'critical factor' for their amplification or damping. In line with this theory, the stabilization of the standing wave regimes for low values of the aspect ratio can be explained by the fact that the disturbances with higher mode number (low aspect ratio) propagate faster than those with smaller m (high aspect ratio) and hence have less time to interact and grow and determine the transition from the pulsating regime to the rotating one.

5. CONCLUSIONS

A numerical code based on a three-dimensional control volume method and able to use a non-uniform mesh has been developed which is able to give a three-dimensional and time-dependent simulation of Marangoni flow instability in cylindrical non-isothermal liquid bridges.

Since most of the existing information for high Prandtl numbers comes from experiments and linear stability calculations, a high-Prandtl number liquid ($Pr = 30$) has been considered in the computations.

The numerical results have been analysed and interpreted in the general context of the bifurcations theory.

The numerical calculations show, according to available experimental results and according to linear stability results, that the lower the aspect ratio is, the higher the critical wavenumber and the more complex the flow field structure is. The empirical correlation $2mA = 1.6$ between the azimuthal wavenumber and the aspect ratio has been found which is almost identical to that one obtained by several experimental investigators for high-Prandtl liquid zones.

Owing to the cylindrical geometry of the floating zone, two different modes for oscillatory flow pattern are principally possible, one being an asymmetric mode and the other a symmetric mode.

The main criterion for the occurrence of symmetric or asymmetric modes is the aspect ratio. A characteristic feature of the asymmetric basic mode $m = 1$ is a periodically 'staggering ring' of vortex core of the toroidal flow pattern on a meridian section of the floating zone and also a periodically tilting branching streamline that divides the two vortices in the generic meridian plane. For the symmetric basic mode two vortices on the meridian plane are moving up and down simultaneously, and accordingly the tilting of the branching streamline disappears.

Standing wave and travelling wave regimes have been observed and depicted in detail.

In the pulsating regime the temperature disturbances 'pulsate', i.e. the cold surface spots grow in the axial direction during the shrinking of the hot spots and vice versa, but the azimuthal positions of these extrema do not change. According to the presence of these surface spots, convective cells are formed in the planes orthogonal to the liquid bridge axis, their number depending on the azimuthal wavenumber. These cells change periodically their sense of rotation and their intensity. The behaviour of the surface spots has been directly related to the motion of the toroidal vortex centreline, whose shape is distorted in the axial direction. The pulsating behaviour of the temperature field in the generic section has been explained considering that the displacement up and down of the toroidal convection roll is coupled to displacement out and in, respectively, with respect to the axis of symmetry of the zone.

The behaviour of the azimuthally travelling regime has been explained in detail too.

In this case the surface temperature spots do not change their intensity and rotate around the perimeter of the liquid bridge. The vortex cells in the section orthogonal to the axis do not change their sense of rotation and their strength is constant in time (the cells never vanish). The time-dependent behaviour of the velocity field is simply characterized by a full rotation of the entire flow pattern in the azimuthal direction.

The numerical results indicate that, close to the onset of instability, the instability is properly described by the standing wave model, but far enough from the transition to time dependence, the oscillatory field is characterized by a wave travelling in the azimuthal direction.

The numerical results pointed out that the transition from one regime to the other depends on the aspect ratio of the liquid bridge. In particular, it was found that the azimuthal standing wave regime is more stable and lasts for a long time for low aspect ratios.

A detailed description of the disturbances and in particular of their azimuthal wavenumber, velocity of propagation and time of growth has been given.

The transition from pulsating regime to rotating regime has been explained in terms of the velocity of propagation of the disturbances in the liquid since this velocity is function of the aspect ratio and of the Marangoni number.

ACKNOWLEDGMENTS

This work is part of the PhD thesis of M. Lappa. The authors would like to thank the Italian Aerospace Research Centre (CIRA), which allowed the numerical calculations on the Silicon Graphics Power Challenge Parallel Supercomputer.

REFERENCES

1. Chun CH, West W. Experiments on the transition from the steady to the oscillatory Marangoni convection of a floating zone under reduced gravity effect. *Acta Astronautica* 1979; **6**: 1073–1082.
2. Chun CH. Experiments on steady and oscillatory temperature distribution in a floating zone due to the Marangoni convection. *Acta Astronautica* 1980; **7**: 479–488.
3. Preisser F, Schwabe D, Scharmann A. Steady and oscillatory thermo capillary convection il liquid columns with free cylindrical surface. *Journal of Fluid Mechanics* 1983; **126**: 545–567.
4. Velten R, Schwabe D, Scharmann A. The periodic instability of thermocapillary convection in cylindrical liquid bridges. *Physics and Fluids A* 1991; **3**: 267–279.
5. Frank S, Schwabe D. Temporal and spatial elements of thermocapillary convection in floating zones. *Experiments in Fluids* 1998; **23**: 234–251.
6. Monti R. On the onset of the oscillatory regimes in Marangoni flows. *Acta Astronautica* 1987; **15**: 557–560.
7. Petrov V, Schatz MF, Muehlner KA, Van Hook SJ, McCormick WD, Swift JB. Experimental control of thermocapillary convection in a liquid bridge. In *Third Microgravity Fluid Physics Conference*, NASA CP 3338, 1996; 487–492.
8. Muehlner KA, Schatz MF, Petrov V, McCormick WD, Swift JB, Swinney HL. Observation of helical traveling-wave convection in a liquid bridge. *Physics and Fluids* 1997; **9**(6): 1850–1852.
9. Schwabe D, Hintz P, Frank S. New features of thermocapillary convection in floating zones revealed by tracer particle accumulation structures. *Microgravity Science and Technology* 1996; **9**: 163–168.
10. Rupp R, Muller G, Neumann G. Three dimensional time dependent modelling of the Marangoni convection in zone melting configurations for GaAs. *Journal of Crystal Growth* 1989; **97**: 34–41.
11. Xu JJ, Davis SH. Convective thermocapillary instabilities in liquid bridges. *Physics and Fluids* 1984; **27**: 1102–1107.
12. Shen Y, Neitzel GP, Jankowsky DF, Mittelmann HD. Energy stability of the thermocapillary convection in a model of the float zone crystal-growth process. *Journal of Fluid Mechanics* 1990; **217**: 639–660.
13. Neitzel GP, Law CC, Jancowski DF, Mittelmann HD. Energy stability of thermocapillary convection in a model of the float-zone crystal-growth process. *Physics and Fluids A* 1991; **3**: 2841–2846.
14. Neitzel GP, Chang KT, Jancowski DF, Mittelmann HD. Linear stability of thermocapillary convection in a model of the float-zone crystal-growth process. *Physics and Fluids A* 1992; **5**: 108–114.
15. Kuhlmann HC. Thermocapillary instabilities in cylindrical liquid bridge. In *Proceedings VIIIth European Symposium on Materials and Fluid Sciences in Microgravity*, Brussels, Belgium, 12–16 April, ESA SP-333, 1992; 79–83.
16. Kuhlmann HC, Rath HJ. Hydrodinamic instabilities in cylindrical thermocapillary liquid bridges. *Journal of Fluid Mechanics* 1993; **247**: 247–274.
17. Chen G, Roux B. Bifurcation analysis of thermocapillary convection in cylindrical liquid bridges. ELGRA Meeting, Madrid, December 1994. *ELGRA News* 1995; **19**: 54.
18. Chen QS, Hu WR. Influence of liquid bridge volume on instability of floating half zone convection. *International Journal of Heat and Mass Transfer* 1998; **41**: 825–837.

19. Savino R, Monti R. Oscillatory Marangoni convection in cylindrical liquid bridges. *Physics and Fluids* 1996; **8**: 2906–2913.
20. Monti R, Savino R, Lappa M. Oscillatory thermocapillary flows in simulated floating zones with time-dependent boundary conditions. *Acta Astronautica* 1997; **41**: 863–875.
21. Monti R, Savino R, Lappa M, Fortezza R. Scientific and technological aspects of a sounding rocket experiment on oscillatory Marangoni flow. *Space Forum* 1998; **2**: 293–318.
22. Lappa M, Savino R. Parallel solution of three-dimensional Marangoni flow in liquid bridges. *International Journal for Numerical Methods in Fluids* 1999; **31**: 911–925.
23. Fletcher CAJ. *Computational Techniques for Fluid Dynamics*. Springer: Berlin, 1991.
24. Rybicki A, Florian JM. Thermocapillary effects in liquid bridges. I. Thermocapillary convection. *Physics and Fluids* 1987; **30**: 1956–1972.
25. Wanschura M, Shevtsova V, Kuhlmann HC, Rath HJ. Convective instability mechanism in thermocapillary liquid bridges. *Physics and Fluids A* 1995; **5**: 912–925.
26. Kuhlmann HC, Rath HJ. On the interpretation of phase measurements of oscillatory thermocapillary convection in liquid bridges. *Physics and Fluids A* 1993; **5**(9): 2117–2120.
27. Monti R, Albanese C, Carotenuto L, Castagnolo D, Ceglia E. First results from 'onset' experiment during Spacelab Mission D-2. In *Proceedings of the Norderney Symposium on Scientific Results of the German Spacelab Mission D2*, Sahm PR, Keller MH, Schiewe B (eds), 1995; 247–258.
28. Yasushiro S, Sato T, Imaishi N. Three dimensional oscillatory Marangoni flow in half-zone of $Pr = 1.02$ fluid. *Microgravity Science and Technology* 1998; **11**: 1–15.

